

MINISTRY OF EDUCATION



**TECHNICAL UNIVERSITY**

OF CLUJ-NAPOCA, ROMANIA

**FACULTY OF AUTOMATION AND COMPUTER SCIENCE  
AUTOMATION DEPARTMENT**

# **MODELLING AND CONTROL OF DRUG DELIVERY SYSTEMS IN GENERAL ANAESTHESIA**

DIPLOMA THESIS

Graduate: **Andreea-Raluca DAFINOIU**

Supervisor: **Conf. Dr. Ing. Ioana NAȘCU**

**2024**



**TECHNICAL UNIVERSITY**

OF CLUJ-NAPOCA, ROMANIA

**FACULTY OF AUTOMATION AND COMPUTER SCIENCE  
AUTOMATION DEPARTMENT**

DEAN,

**Prof. dr. ing. Mihaela DÎNSOREANU**

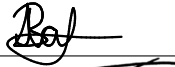
HEAD OF DEPARTAMENT,

**Prof. dr. ing. Honoriu VĂLEAN**

Graduate: **Andreea-Raluca DAFINOIU**

**MODELLING AND CONTROL OF DRUG DELIVERY SYSTEMS IN GENERAL  
ANAESTHESIA**

1. **Project proposal:** The main objective of this work is to explore the modelling and control of general anaesthesia, with the ultimate goal of implementing optimized drug delivery systems. These systems aim to ensure safer and more comfortable surgeries for patients, while also reducing the workload of anaesthesiologists.
2. **Project contents:** Presentation page, introduction, bibliographic research, analysis and theoretical foundation, detailed design, implementation and results, conclusions.
3. **Place of documentation:** Technical University of Cluj-Napoca, Automation Department
4. **Consultants:**
5. **Data of issue of the proposal:** December 18, 2023
6. **Data of delivery :** July 9, 2024

Graduate: 

Supervisor: 



## SUMMARY

of Diploma Thesis entitled:

**Modelling and Control of Drug Delivery Systems in General Anaesthesia**

Graduate: **Andreea-Raluca DAFINOIU**

Supervisor: **Conf. Dr. Ing. Ioana NAȘCU**

### 1. Requirements:

- Create models for hypnosis and neuromuscular blockade.
- Develop and compare control strategies for both hypnosis and neuromuscular blockade.

### 2. Proposed Solutions:

- Implemented the models and control strategies using Matlab and Simulink.
- Used pharmacokinetic-pharmacodynamic (PKPD) models and developed PID, IMC-PID, and MPC control strategies for hypnosis.
- Used Wiener models and developed PID and IMC-PID control strategies for neuromuscular blockade.

### 3. Results Obtained:

- For hypnosis, aimed for a Bispectral Index value of 50 with a maximum settling time of 4-5 minutes.
- For neuromuscular blockade, targeted a 10% amplitude of the first twitch after stimulation with a maximum settling time of 60 minutes.

### 4. Testing and Validation:

- Developed models based on a dataset of patients.
- Designed controllers using a nominal patient model and tested them on additional patients.
- Analyzed and compared the obtained results.



**5. Personal Contributions:**

- Developed and optimized the proposed control strategies using Matlab and Simulink, focusing on achieving desired performances for hypnosis and neuro-muscular blockade..
- Conducted testing and validation on patient data to ensure robustness of the developed controllers.

**6. Documentation Sources:**

- Scientific articles from IEEE.
- Online documentation from Science Direct, the National Center for Biotechnology Information (NIH, USA), and National Instruments.

Graduate:

Supervisor:

# Contents

<b>Chapter 1 Introduction - Project Context</b>	<b>1</b>
1.1 Project Context . . . . .	1
1.1.1 General Anaesthesia . . . . .	1
1.1.2 Modelling and Control in Anaesthesia . . . . .	2
1.2 Scope and Objectives . . . . .	4
1.3 Outline . . . . .	5
<b>Chapter 2 Bibliographic Research</b>	<b>7</b>
<b>Chapter 3 Analysis and Theoretical Foundation</b>	<b>13</b>
3.1 PKPD models . . . . .	13
3.1.1 PK models . . . . .	13
3.1.2 PD models . . . . .	13
3.2 Wiener Models . . . . .	15
3.3 Control . . . . .	15
3.3.1 PID Tuning with FRTool . . . . .	16
3.3.2 Internal Model Control Tuning . . . . .	17
3.3.3 Model-Predictive Control Tuning . . . . .	20
<b>Chapter 4 Detailed Design, Implementation and Results</b>	<b>24</b>
4.1 Hypnosis Implementation . . . . .	24
4.1.1 PID Controller Tuned With FR Tool . . . . .	28
4.1.2 IMC Tuning . . . . .	31
4.1.3 MPC Tuning . . . . .	37
4.1.4 Controllers Response to Perturbation . . . . .	39
4.2 Neuromuscular Blockade Implementation . . . . .	45
4.2.1 PID Controller Tuned With FR Tool . . . . .	46
4.2.2 IMC Tuning . . . . .	49
<b>Chapter 5 Conclusions</b>	<b>53</b>
5.1 Contributions and Achievements . . . . .	53
5.2 Future Developments . . . . .	54
<b>Bibliography</b>	<b>55</b>
<b>Appendix A Published Papers</b>	<b>59</b>

# **Chapter 1. Introduction - Project Context**

Every day, a staggering number of individuals undergo major surgeries worldwide. According to [1], there is a minimum estimated need of 321 million surgical procedures annually, with an unmet need of 143 million cases. In the realm of surgical procedures, anaesthesia plays a crucial role in ensuring the well-being of patients on the operating table. Its indispensable role cannot be debated, as it directly impacts the health and safety of individuals undergoing medical interventions.

## **1.1. Project Context**

### **1.1.1. General Anaesthesia**

The roots of anaesthesia can be traced back to ancient times. As discussed by Dumas [2], ancient Egyptians used substances such as Indian hemp and poppy juice to cause drowsiness in patients before surgical procedures, as well as the Scythians achieved a form of intoxication by inhaling the vapour of a specific type of hemp. By the seventeenth century, the use of narcotic drugs gained popularity for inducing anaesthesia and alcohol was employed similarly. However, a significant movement arrived only in 1818 with the introduction of sulfuric ether as a form of inducing anaesthesia.

The primary goal of general anaesthesia is to keep the unconsciousness of the patient undergoing surgery intervention. While under anaesthesia, individuals experience a state of insensitivity to pain and have no memory of painful stimuli associated with the surgery. The maintenance of life is ensured through regulation of nervous, respiratory and cardiac systems. Moreover, the role of the anaesthesiologist is crucial in continuously monitoring throughout the surgery. This involves thoughtful observations of changes in vital body functions, including heart rate, blood pressure, breathing, heart rhythm and body temperature. Technology also plays an important role in the monitoring process, enabling real-time assessment of organ functions. This approach ensures the safety and the success of surgical procedures [3].

Modern general anaesthesia is characterized by the triad of hypnosis, analgesia and muscle relaxation. Hypnosis achieves a state of unconsciousness, ensuring patients don't sense any painful stimuli during surgery. Analgesia represents the absence of pain, used for blocking the perception of painful sensations. Muscle relaxation is facilitated by neuromuscular blocking drugs, which interrupt the signal transmission between the nerves and skeletal muscles, preventing the muscle contraction during the surgery. A requisite balance among the three components of anaesthesia is essential during surgery. This balance ensures a consistent execution of the procedure, minimizing any potential harm to the patient [3].

### 1.1.2. Modelling and Control in Anaesthesia

Automating the anaesthesia process can be seen as a challenge as it requires precise patient modelling and effective control strategies to optimize drug dosages while ensuring the patient's safety [4].

As is common knowledge, patients present unique characteristics, resulting in variations in drug concentration from patient to patient, even if administered the same drug dosage during the surgery. This motivated the development of PKPD models, which are based on the principle "what the body does to the drug" versus "what the drug does to the body". The PK model addresses "what the body does to the drug", involving modelling drug diffusion through body tissues and the drug flow in the blood. Contrastingly, the PD model captures "what the drug does to the body", describing the relationship between drug concentration and observed clinical effects, such as patient vital signs. PK models are typically expressed by compartment models, as PD models are characterized by the nonlinear Hill equation [4], [5].

Another model used in patient modeling is the Wiener model, as developed in [6] and [7]. This model is structured as a block-oriented model, comprising two parts: a linear dynamic component and a nonlinear static component. It has been used in various applications to represent nonlinear systems, such as in neuromuscular blockade.

From a control engineering perspective, several control strategies have been developed for each component of the triad: hypnosis, analgesia and muscle relaxation. Implementing control in drug administration has come with several benefits, for instance lowering costs by reducing medication volume per intervention and faster recovery time with fewer postoperative side effects [8].

Despite these advantages, the anaesthesiologist remains a key component in the control process. With a broader view than the controller, including access to information about the patient's vital signs (e.g. heart rate, blood pressure, breathing, body temperature), the anaesthesiologist can intervene at any time if necessary to adapt decisions made by the controller [9].

The focus of this paper is on hypnosis and neuromuscular blockade. Before starting the modelling and the control design process, it is necessary to understand what they consist of, as well as the expected performances in the surgery room.

## Hypnosis

Hypnosis is the state of unconsciousness in which the patient doesn't sense any painful stimuli during the surgery. One of the most used drugs to induce hypnosis is propofol, due to its large absorption and rapid elimination by the body. Monitoring the depth of anaesthesia is done through the observation of the BIS value (Bispectral Index), which is determined based on electroencephalogram waveforms [10]. Multiple electrodes are applied on the patient's scalp to measure the brain's electrical activity (Figure 1.1), with the measurement instrument then transforming the raw data into the dimensionless BIS value [11].

As it can be seen in Figure 1.2, the BIS value ranges from 0 to 100, where 0 indicates a flat line in the EEG and 100 indicates full awkeness. During surgery, it's important to maintain the BIS value within the range of 40 to 60 . If the BIS value is under 40, the risk of experiencing cardiovascular or respiratory collapse and postoperative delirium increases, as if it's above 60, the patient may recall and respond to commands, indicating awareness of the surgical intervention [13].

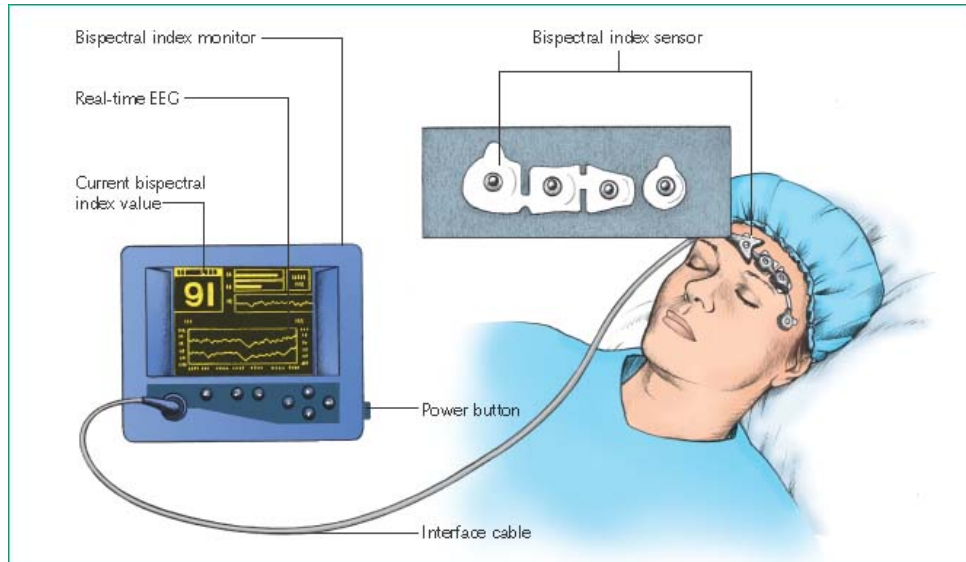


Figure 1.1: BIS Monitoring schema. Source: [12]

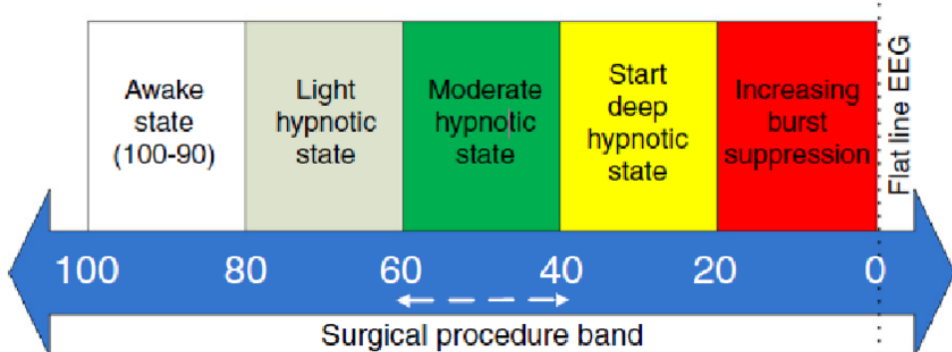


Figure 1.2: BIS index range and patient's state. Source: [3]

The hypnosis process can be divided into three stages: induction phase, maintenance phase and emergence phase. The induction phase usually lasts about 4-5 minutes, during which the BIS value is drawn from 100 to 50. In the maintenance phase, the BIS value must be ensured within the 40-60 range as aforementioned. During the emergence phase, administration of propofol is stopped, starting the patient's awakening [13].

### **Neuromuscular blockade**

Neuromuscular blockade is used in anaesthesia to obstruct muscle contraction during surgery, aiding endotracheal intubation and mechanical ventilation [6]. Quantitative monitoring is required in order to minimize the impact of residue of the neuromuscular block, therefore optimizing postoperative recovery. Among the potential complications we enumerate pneumonia, respiratory failure, hypoxic episodes or the necessity of airway support [14].

The depth of neuromuscular blockade is measured using the Train-of-Four (TOF) Watch device, a widely used method for monitoring muscle relaxation. This involves applying four consecutive 2Hz stimuli to a muscle group, causing muscle contraction with each stimuli (see Figure 1.3). The amplitude of the first twitch (T1) is measured as the

output [15]. Since neuromuscular blocking agents (NMBAs) are usually administered continuously, careful attention is needed to avoid irrational dosage, which can lead to overdosing and postoperative complications [16].

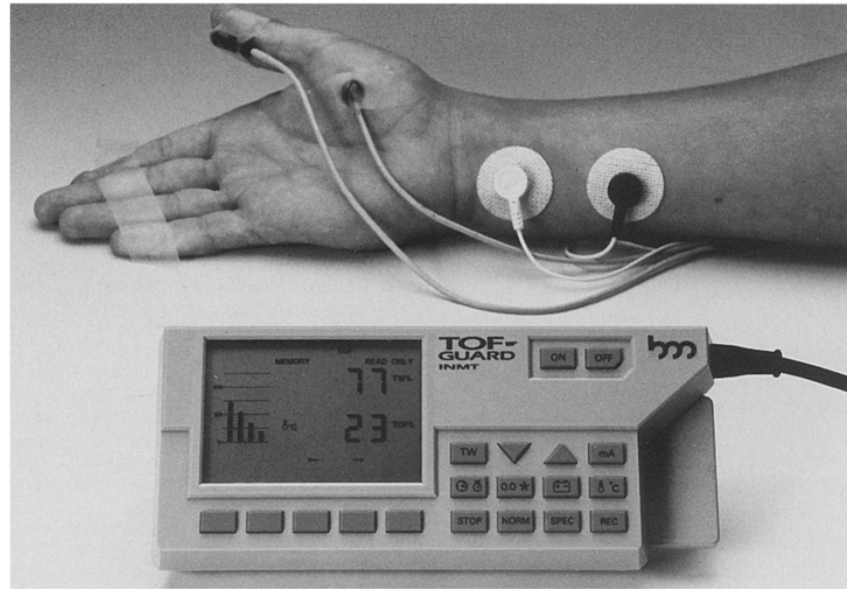


Figure 1.3: TOF Guard Monitor. Source: [17]

In Figure 1.4, response to TOF stimulation is depicted. After the injection of the blocking agent, the neuromuscular blockade goes through three stages: intense blockade, where no response to stimulation can be seen; surgical blockade, when the patient starts to respond to one stimulus, corresponding to a 90-95% degree of relaxation; and the recovery.

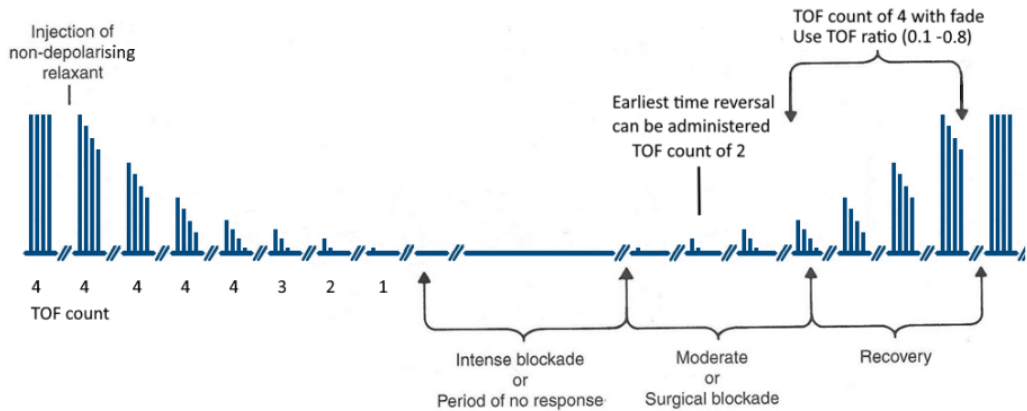


Figure 1.4: Response to TOF stimulation. Source: [18]

## 1.2. Scope and Objectives

Developing a control strategy implies multiple steps, including modelling, designing of the control law, implementation, testing and validation [19]. In medical applications,

this process can rise some difficulties, starting from developing an appropriate mathematical model that can accurately capture patient dynamics during the intervention, as well as parameter variability that exists from patient to patient [3].

The Figure 1.5 shows the automated anaesthesia process, seen as a repetitive loop. Initially, the controller receives the desired set-point and computes the optimal drug dosage for the patient, that will be administered to the patient through an infusion pump. Also, as mentioned before, the presence of an anaesthesiologist allows manual adjustments on the decisions made by the controller. Continuous monitoring of the vital signs throughout the surgical process is essential to ensure the patient's safety.

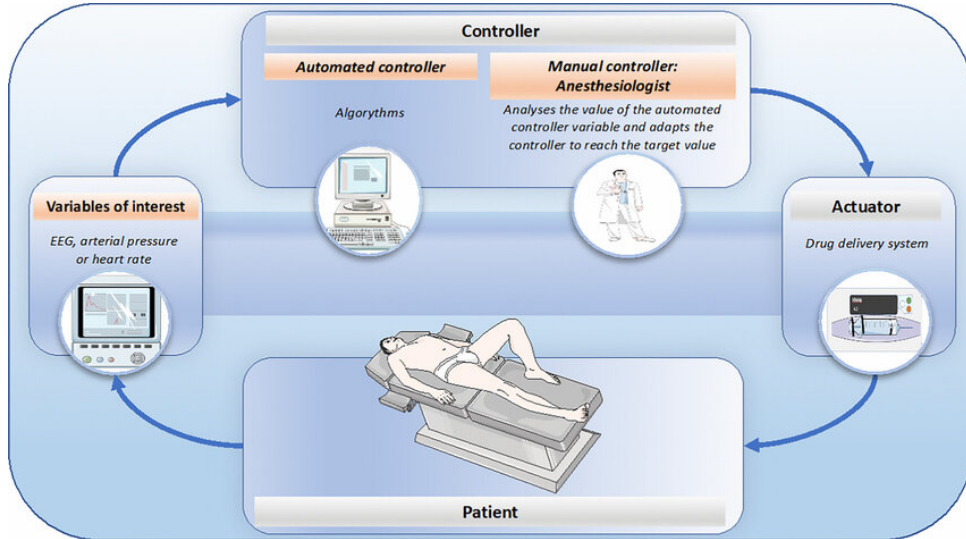


Figure 1.5: Automated control of anaesthesia. Source: [20]

The main objectives of this paper are to develop and compare control strategies for anaesthesia management, specifically focusing on hypnosis and neuromuscular blockade. The specific goals include:

- **Developing control strategies for hypnosis:** Design and implement three control strategies - PID, IMC and MPC - based on a nominal patient. The aim is to ensure these controllers effectively maintain the desired level of hypnosis during surgery.
- **Developing control strategies for neuromuscular blockade:** Design and implement two control strategies - PID and IMC - based on a nominal patient. The goal is to maintain the appropriate level of muscle relaxation needed for surgical procedures.
- **Testing and performance comparison:** Test and compare the performance of the developed controllers on a set of patients to assess their effectiveness and robustness. This includes conducting simulations to observe how well each control strategy performs.
- **Test disturbance response of the controller developed for hypnosis:** Generate a disturbance signal and compare how each of the three developed controllers for hypnosis respond to this disturbance. This test will help evaluate the ability of each controller to maintain the desired level of hypnosis despite disturbances.

### 1.3. Outline

The paper is organized as follows: Chapter 2 Presents the bibliographic research on the modeling and control of hypnosis and neuromuscular blockade, discussing methods

developed and tested in recent years and their outcomes. Chapter 3 provides a theoretical background, explaining the development of the models and the mathematical foundation behind each control strategy. Chapter 4 Details the design and implementation of the model and control strategies, and discusses the simulation results. Chapter 5 concludes the paper.

## Chapter 2. Bibliographic Research

In terms of modelling and control of anaesthesia, developments have been made since the 1960s and 1970s [21]. Nowadays, the PKPD models reliably capture the patient dynamics, while control methods have evolved from the traditional PID controller to the modern predictive and adaptive approaches. In this chapter, recent research that present the current state of these developments will be discussed. For hypnosis, it covers results on PID-based control, IMC, fuzzy control, MPC, and sliding mode control. For neuromuscular blockade, it presents findings on PID, IMC, SMMAC, and ESPAC.

In the study [22], a PID-based model was evaluated on nine patients divided into three subgroups as follows: the first received drug boluses via Graseby 3400 pumps without additional manual interventions; the second used the same pumps with the option for anaesthesiologist intervention; and the third utilized Alaris GH pumps without anaesthesiologist intervention. The paper details the controller's performance during both the induction and maintenance phases of anaesthesia. In subgroups where the anaesthesiologist did not intervene, the results were satisfactory: rapid induction of anaesthesia depth in all patients (approximately 1.15 minutes), with the BIS maintained within the recommended range for 80% of the time. Although two patients exceeded the recommended range during maintenance, the controller successfully rejected the disturbances that led to this effect. For the subgroup where the anaesthesiologist could intervene, the controller effectively managed disturbances caused by additional boluses. However, the induction time was longer compared to the other subgroups (around 3 minutes).

An IMC control method was developed in [13]. The controller design included a second-order low pass filter and introduced two additional poles to ensure that the controller's transfer function is proper. These two poles were tuned using a particle swarm optimization algorithm with the help of Matlab Global Optimization Toolbox. This algorithm operates without noise, and the filter was not considered in this process. It was observed that the optimal result occurred when the two poles were equal and smaller for the load disturbance rejection task. For the filter's time constant, the approach involves incrementing its value starting from 0 and computing the performance decay ratio index for each value. This was done by finding the maximum difference between IAE (integrated absolute error) for each patient in the presence of noise and the IAE value without noise, divided by the latter. The robustness of the controller was tested using the Monte Carlo method, which involved randomly generating a set of 100 patients. The results showed that the control requirements were satisfied for both the set of 100 patients and the original set of 12 patients (on which the controller was tuned), meeting clinical standards. For the set of 12 patients, there was no overshoot or undershoot in the BIS value, and the control signal was smooth, stabilizing quickly. For the set of 100 patients, a small undershoot occurred in some cases, but the value never dropped below 40.

Another approach to control hypnosis is fuzzy control, as implemented in [23]. The authors began by defining input variables for patient state classification: the difference between the measured BIS value and the target BIS value ( $E$ ), the change of  $E$  over 15 seconds ( $\delta E$ ), and the predicted BIS error ( $pE$ ), which relies on the propofol response to predict the control error for the next 60 seconds. The fuzzy classification of the patient state involved nine kernels for  $E$  and  $pE$ , and three kernels for  $\delta E$ . Defuzzification was performed to associate the patient state with the required drug bolus. The dosing was optimized using the Simulated Annealing method, structured as a three-dimensional minimization problem. Two fuzzy controllers were optimized: one for a BIS target of 60 and another for a BIS target of 40. These controllers were simulated over 1000 episodes, with the targets applied in random order to test their response to intra- and inter-patient variability. Performance was analyzed using the Varvel method, by computing the Performance Error (PE) at each time step for each episode, as well as MDPE for control bias, MDAPE for control accuracy, wobble for inter-patient variability, divergence for control stability, and the controlled metric for the percentage of timesteps the target remained within  $\pm$  BIS target. The MDPE was less than 1%, the MDAPE was approximately 2.5%, wobble was 2.5%, and divergence was 0.002%. These values show effective stabilization of the target, as also reflected by the controlled metric, which was 89.9%.

Controlling the hypnosis was also addressed in MIMO systems, as presented in [24]. This study proposes a DMPC (Distributed Model Predictive Control) control for a hypnosis-hemodynamic combined model. The hemodynamic model has two inputs, Dopamine and Sodium Nitroprusside (SNP, used to lower blood pressure), and two outputs, Cardiac Output and MAP (Mean Arterial Pressure). For the hypnosis model, the three-compartment model was used for the pharmacokinetics and the Hill equation for the pharmacodynamics. A simplified version of the model was used for control purposes, divided into two subsystems: one for hypnosis regulation and the other for hemodynamic control. To simplify, SNP was chosen as the input and MAP as the output for the hemodynamic subsystem. These two subsystems are coupled in a sequential architecture since propofol affects MAP, but SNP does not influence the BIS value. The optimal control signals for both subsystems are computed using a DMPC algorithm, with a control horizon  $N_c = 1$ , a prediction horizon  $N_p = 10$ , propofol constraints  $[0, 3.5]$ , and SNP dosage constraints  $[0, 10]$ . The simulation was conducted on a single patient, with performance tested against a disturbance rejection experiment. It was observed that infusing dopamine in the hemodynamic model negatively influenced the propofol bolus, risking patient awakening. However, the BIS value remained within the recommended range of 40-60, the SNP dosage did not exceed limits, and MAP stayed within the recommended range of 70-100 mmHg.

In the paper [25], a GPC (General Predictive Control) strategy is proposed to optimize the propofol administration at each sample time. Because the internal predictor of the GPC limits the influence of the prediction errors over a larger horizon, the authors are using an external predictor and three filters to make the system more robust. The filters serve different purposes: filtering the high peaks of the measurement noise, ensuring system robustness, and providing the set-point tracking to the control architecture. At each sample time, the GPC minimizes both the cost function and future control effort. A genetic algorithm, applied to a set of 40 elements, optimizes the parameter selection for the controller. The experimental study involved four patients undergoing plastic surgery. The setup included two Alaris GH pumps (one for propofol, the other for remifentanil for analgesia) and a monitor for the anesthesiologist to oversee patient behavior, set BIS

---

targets, switch between induction and maintenance control modes, and transition between manual and automatic control. During the induction phase, the fastest induction time recorded was 1.10 minutes, while the lowest BIS reading was at 23. These rapid BIS changes did not affect hemodynamic variables, as blood pressure (BP) and heart rate (HR) remained within recommended ranges. The propofol bolus administered ranged from 1.91 mg/kg to 2.52 mg/kg, consistent with clinical practice standards. For the maintenance phase, performance metrics such as MDPE, MDAPE, wobble, and patient wake-up times were monitored. The BIS value was maintained within the 40-60 range for 57.78% to 75.05% of the time. The control system effectively managed the anaesthesia without requiring the anaesthesiologist intervention, maintaining appropriate BIS levels and stable blood pressure and heart rate. Nevertheless, additional manual administration was necessary for patient 3 as a prevention to a particular painful part of the surgery, patient 2 experienced an increase in BP, and patient 3 had a sharp rise in BP due to the administration of ephedrine to counteract low BP.

Nonlinear control techniques have been developed for such processes, as presented in the paper [26], in which sliding mode control for depth of anaesthesia regulation is introduced. This approach drives the system's dynamics towards a sliding surface, specifically stabilizing and maintaining the BIS value at 50. The control law has two components: the equivalent control signal, that directs the system towards the given reference based on its current state and parameters, and the discontinuous control signal which handles the disturbances. Simulations were conducted on eight patients, showing that the controller achieves the target of 50 within 70 seconds for most of the patients. Due to high intra- and inter-patient variability, some individuals exhibited the BIS target value, but still remained in the recommended range of 40-60. Additionally, the study investigated whether weight influenced drug concentration, in the same manner that the age does, by comparing the effect of drug concentration between two patients of similar age but different weight (with a 30kg difference). It was observed that the bolus of propofol was comparable for both patients, with a minor difference due to age difference.

The BIS index is not the only method for measuring the depth of anaesthesia during surgery. According to the paper [27] the Auditory Evoked Potential Index (aepEX) offers an alternative way, that might be surpassed than the BIS index. The aepEX can distinctly distinguish between patient consciousness and unconsciousness states and is independent of the anaesthetic drug. While the BIS index is widely used, it is affected by the bolus of anaesthetic drug and presents nonsmooth changes near certain values. Contrastingly, aepEX is computed as the sum of the square roots of the absolute differences between successive 0.56ms segments of the auditory evoked potential waveform in response to a 6.9Hz auditory stimulus.

The main idea in this paper starts from using the relationship between the effect-site concentration and aepEX to estimate the minimum effect-site concentration required to maintain patient unconsciousness. This relationship was studied in patient after the drug induction, using Barr pharmacokinetics parameters for their high accuracy. Two classification conditions were imposed: if the current concentration is less than the minimum effect-site concentration during the unconscious period (or  $aepEX > 56$ ), the patient is considered conscious; if the current concentration is greater than the maximum effect-site concentration during the conscious period (or  $aepEX < 56$ ), the patient is considered unconscious.

During the induction phase, two estimations were defined. One estimation using BIS to estimate the minimum effect-site concentration expressed as:  $c_{e,min} = 0.047c_{BIS,45} +$

$0.87\mu\text{g mL}^{-1}$ , where  $c_{BIS,45}$  is the propofol concentration at which the BIS value decreases by 45% of the maximal effect intensity. The second estimation specifies that if  $aepEX$  drops below 37 within 10 minutes, the minimum effect-site concentration is the one associated with  $aepEX = 37$ ; otherwise, if the  $aepEX$  doesn't drop below 37, it is computed as the concentration at which the  $aepEX$  decreases by 90% of its maximal effect intensity.

For the maintenance phase, two scenarios are considered. If hypnosis is maintained at a deep level, the slope of the pharmacodynamic model is computed over the last 15 minutes within the range  $[c, c + 0.5\mu\text{g mL}^{-1}]$ , where  $c$  is the current concentration. Two conditions must be met:

- $aepEX_{slope} < -5\text{mL mg}^{-1}$
- $aepEX_1 > aepEX_2$

where these values represent the average values within the range  $[c, c + 0.5\mu\text{g mL}^{-1}]$ , respectively  $[c + 0.5\mu\text{g mL}^{-1}, \text{inf}]$ . If hypnosis is not kept at a deep level and is acceptable, then the minimum concentration is estimated using the earlier procedure. If the hypnosis level is not acceptable, then the minimum effect-site concentration is determined by  $c_{e,min} = c + 0.2\mu\text{g mL}^{-1}$ .

The control method implemented was MPC, with simulations conducted on a set of 13 patients and a nominal one. The MPC action began 10 minutes after the induction of propofol and continued for the next 150 minutes. Results show that the minimum concentration was estimated accurately, maintaining the desired level of hypnosis. Although the effect-site concentration proposed by the authors is approximately 9% less than found in clinical data, the results are satisfactory, achieving a reduction in the amount of administrated drug, while maintaining the desired depth of anaesthesia.

The research paper [28] presents a control strategy for the Target Control Infusion (TCI) system for rocuronium, a drug used to induce muscle relaxation during surgery. To improve the standard TCI, the authors propose an individualized pole placement method. The linear component of the model is expressed as a transfer function  $G(s) = \frac{40\alpha^3}{(s+\alpha)(s+4\alpha)(s+10\alpha)}$ , while the nonlinear component is described by the Hill equation  $R = \frac{r_0^{\gamma}}{1 + \frac{C_e}{EC50}}$ . Here,  $R$  denotes the level of neuromuscular blockade,  $r_0$  is the NMB level when drug concentration is zero, and  $\gamma$  and  $\alpha$  are patient dependent parameters that need to be identified. These parameters are determined during the initial bolus response, where the clinically recommended bolus of  $600 \text{ mg kg}^{-1}$  is administered. Once estimated for each patient, the model is rewritten in a canonical controllable form that will be used in control design. The core of this control strategy is to keep the fastest poles of the linear part (those farthest from the stability limit) and change the slowest pole (closest to the stability limit) to a new value of  $p = -\lambda\tilde{\alpha}$ , where  $\tilde{\alpha}$  is the previously estimated  $\alpha$ . The best tracking results are achieved by keeping  $\lambda$  within the range  $(0, 1]$ . To find the optimal  $\lambda$ , the authors use the total quadratic error and define a cost function, obtaining three values for  $\lambda$ . The results are promising, showing an undershoot in the first 50 minutes of simulation but successfully tracking the reference of 10% after 100 minutes.

In [29], an adaptive control approach is proposed for handling the neuromuscular blockade using atracurium for induction. This control method is based on Switch Multiple Model Adaptive Control (SMMAC) and is validated with actual clinical cases. The model consists of a PKPD model, where the pharmacokinetic part consists of two plasma compartments connected by linear equations, and the pharmacodynamic part is represented by the Hill equation. The control schema includes a set of plant models designed to cover a range of possible system dynamics and a bank of controllers from which the best performances controller is selected. Each controller in the bank has a PID struc-

---

ture, with parameters determined using a dominant-pole placement rule. The system's output is estimated using an ARX model, a mathematical tool that predicts the current output based on past outputs and inputs. This approach is effective for adaptive control as it forecasts the patient's response by analyzing previously reactions of the patient to the drug and current dosage, allowing continuous adjustment for accurate control action. Simulations were conducted on a bank of 100 nonlinear models, followed by physical tests in elective surgeries. The simulations showed promising results, with the neuromuscular blockade stabilizing after approximately 50 minutes and presenting a minor, insignificant undershoot during the induction phase. In the elective surgeries case, the controller was implemented in a computer that received the muscle relaxation level signals via the RS 232C port and updated the drug dose delivered by the pump at every 20 s. The surgical results confirmed the simulations, presenting good performances by successfully stabilizing patient dynamics without imposing prior restrictions on the bank of models and controllers.

In the paper [6], a strategy for modeling neuromuscular blockade during general anesthesia is presented. The authors base their model on a Wiener model, which consists of a linear dynamic block represented by a third-order transfer function and a static nonlinear block described by the Hill equation. This model was identified using clinical data collected during surgeries in which patients received boluses of atracurium to induce neuromuscular blockade. Muscle relaxation was assessed by applying four supra-maximal electrical stimuli and analyzing the response with a TOF-Watch Sx device. The authors focused on the first twitch of the TOF response for model identification and control, as it was found to be smooth and sufficiently descriptive. The resulting model, initially a third-order transfer function, was simplified to a second-order transfer function. Parameters for the nonlinear Hill equation were identified using the nonlinear least-squares method, with the input being the estimated effect-site concentration from the linear model and the output being the first twitch. The final results demonstrate that the developed model provides an excellent fit.

Based on the model aforementioned, two control methods, PID and ESPAC, were proposed in [30]. The PID controller was tuned using a frequency-response tool, which allows the user to define design specifications such as overshoot, settling time, and robustness. These specifications are then converted into graphical constraints, making it easier to determine if the designed controller meets the requirements. Simulations of the PID controller yielded promising results: for one patient, the neuromuscular block was induced within 60 minutes with no overshoot. However, due to intra- and inter-patient variability, another patient experienced an increased settling time of 110 minutes and response oscillations. To address these issues, the authors proposed an adaptive predictive control method, specifically ESPAC (Extended Prediction Self-Adaptive Control). This strategy predicts the system's future output based on two effects: one accounting for past control actions, future control scenarios, and predicted disturbances, and the other optimizing future control actions. By minimizing a cost function, the optimal control input is computed. The results were favorable, with the administered drug amount staying below the imposed constraint (mean infusion rate approximately 0.0089 mg/sec versus an upper limit of 0.33 mg/sec). ESPAC demonstrated better settling time and minimal undershoot. The authors noted a trade-off in optimizing the prediction horizon: increasing it reduces overshoot but increases settling time.

Studies addressing multivariable systems can be found in the literature, such as the work presented in [31]. This study proposes a interval type-2 fuzzy logic controller

(IT2-FLC) for automatic control of anaesthesia. The multivariable model contains muscle relaxation induced by atracurium and depth of anaesthesia induced with isoflurane. The atracurium model is a compartmental model with a nonlinear Hill equation,  $G_{11}(s) = \frac{k_1 e^{-\tau_1 s} (1+T_4 s)}{(1+T_1 s)(1+T_2 s)(1+T_3 s)}$ , while the isoflurane model is a first-order transfer function, describing the relationship between the drug concentration and the mean arterial blood pressure (MABP),  $G_{22}(s) = \frac{k_2 e^{-\tau_2 s}}{(1+T_5 s)}$ . It was clinically shown that the atracurium's interaction with MABP is insignificantly small, but isoflurane's interaction with the neuromuscular blockade is significant and modeled as  $G_{12}(s) = \frac{k_4 e^{-\tau_3 s}}{(1+T_6 s)(1+T_7 s)}$ . The overall control model is summarized as:

$$\begin{bmatrix} paralysis \\ \Delta MABP \end{bmatrix} = \begin{bmatrix} G_{11}(s) & G_{12}(s) \\ 0 & G_{22}(s) \end{bmatrix} \begin{bmatrix} U1 \\ U2 \end{bmatrix}$$

IT2-FLC controllers are used due to their effectiveness in handling uncertainties, such as those arising from patient variability. This controller incorporates four components: fuzzifier, inference engine, rules and defuzzifier. A genetic algorithm optimizes the parameters of the fuzzy logic controller's membership functions. Simulations conducted on a nominal patient showed that the controller used clinically recommended drug dosages to induce the muscle relaxation and hypnosis, while maintaining a constant blood pressure. Additional simulations, using models with parameters generated by the Monte-Carlo method to account for patient variability, showed that atracurium dosage increased while the isoflurane dosage decreased. Nonetheless, the controller successfully maintained the desired levels of muscle relaxation and blood pressure. In all simulations, the output responses exhibited no overshoot or undershoot.

## Chapter 3. Analysis and Theoretical Foundation

In this chapter, general concepts and approaches for modelling and controlling the anaesthesia process are introduced. First, models for hypnosis and neuromuscular blockade are presented, specifically PKPD and Wiener models. Further, the implemented control methods are outlined, with their results discussed in the next chapter.

### 3.1. PKPD models

The PKPD model used in this paper is the same with the one developed in [4].

#### 3.1.1. PK models

Pharmacokinetics is generally defined as the interaction between a drug and the body, describing drug distribution, its elimination and effect-site concentration after its administration. These models are often multi-compartmental, especially for intravenously administered drugs, such as propofol.

The model used in this paper is a three-compartmental model with effect-site compartment and it can be seen in the Figure 3.1.

Typically, the central compartment represents the fast-acting compartment (blood), while the other two represent slow-acting compartments (muscle and fat). The effect-site compartment is hypothetical compartment that show the transport dynamics of the drug to the effect location.

The PK model is expressed by the next set of equations:

$$\begin{cases} \frac{dC_1}{dt} = -[k_{10} + k_{12} + k_{13}]C_1 + k_{21}C_2 + k_{31}C_3 + \frac{u(t)}{V_1} \\ \frac{dC_2}{dt} = k_{12}C_1(t) - k_{21}C_2(t) \\ \frac{dC_3}{dt} = k_{13}C_1(t) - k_{31}C_3(t) \end{cases} \quad (3.1)$$

- $C_1$  - concentration in the fast compartment
- $C_2, C_3$  - concentrations in the slow compartments
- $k_{ij}$ ,  $i = 1:3$ ,  $i \neq j$  - rate constants for distribution between compartments (they depend on age, gender, height and weight)
- $V_1$  - drug infusion input

#### 3.1.2. PD models

The PD model represents the dose-effect response, given by the Hill equation. This static nonlinear function describes the relationship between drug concentration ,  $C$ , and

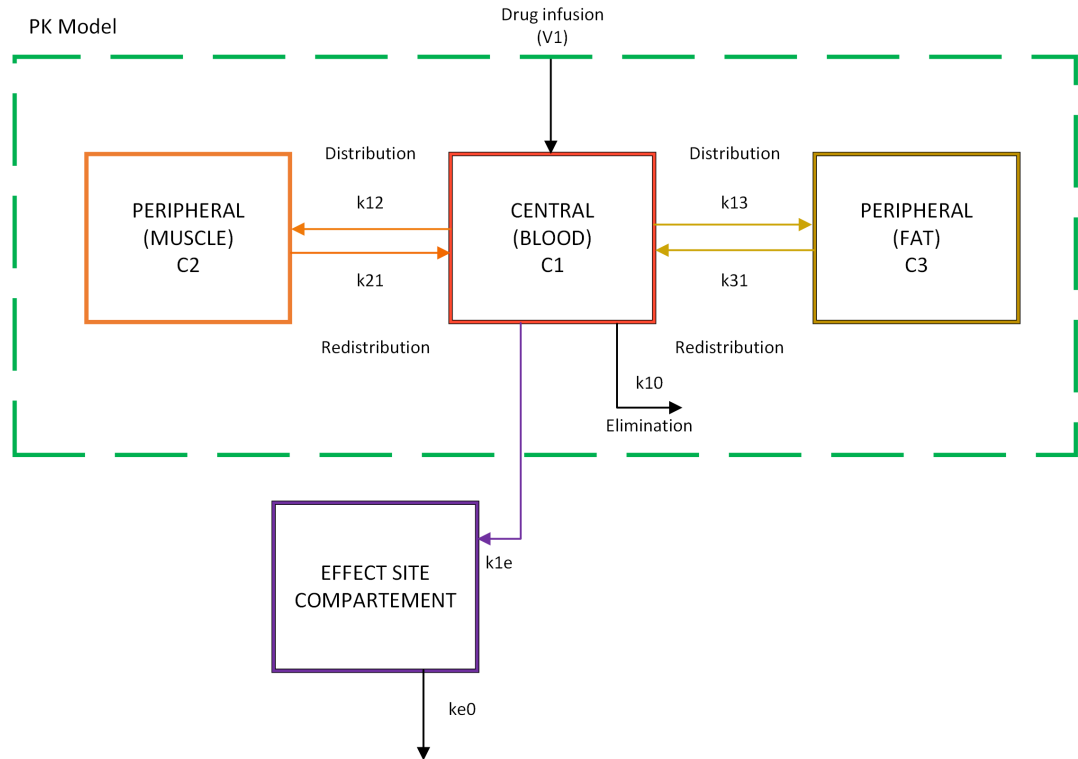


Figure 3.1: Pharmacokinetic three-compartment model

drug effect  $E$ .

$$E = E_0 - E_{\max} \cdot \frac{C_e(t)^\gamma}{C_e(t)^\gamma + C_{50}^\gamma} \quad (3.2)$$

- $E_0$  - the effect when the drug concentration equals 0
- $E_{\max}$  - maximum possible effect
- $C_e$  - effect-site compartment concentration
- $C_{50}$  - drug concentration for which 50% of the maximal effect is obtained
- $\gamma$  - Hill coefficient of sigmoidicity (steepness of the curve when  $C_e = C_{50}$ )

To compensate the nonlinearity introduced by the Hill function within the pharmacodynamic model, a parameter scheduling technique is used, respectively the inverse of Hill function. This parameter transforms the measured BIS values into a  $C_e$  value, used as feedback for the controller. Afterwards, the controller determines the appropriate drug infusion rate by comparing the estimated  $C_e$  value from the inverse function with the reference value. Similarly, the reference BIS value is converted into a corresponding  $C_e$  value using the inverse Hill function to provide a suitable reference for the controller. The inverse of the Hill curve is defined as follows:

$$C_e(t) = EC50 \left( \frac{E_0 - BIS(t)}{E_{\max} - E_0 + BIS(t)} \right)^{\frac{1}{\gamma}} \quad (3.3)$$

### 3.2. Wiener Models

The Wiener model detailed below is the one from [6].

The relationship between the neuromuscular blocking agent given to the patient and the dose effect during general anaesthesia can be modeled by a Wiener structure, depicted in the figure below.

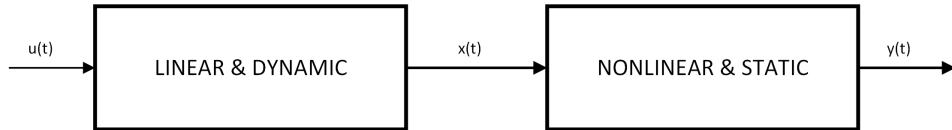


Figure 3.2: Wiener model structure

In this model, the linear part is obtained from the PKPD three-compartmental model (Equation 3.1). The effect-site compartment is modeled using a sigmoid network function, being related to the first twitch  $T_1$ . The resulting model is a third order transfer function, which is further approximated with a second order transfer function:

$$G(s) = \frac{\frac{K}{p}(s + z)}{s^2 + 2\zeta\omega_n s + \omega_n^2} \quad (3.4)$$

where  $K, p, z, \zeta, \omega_n$  are estimated parameters for each patient.

The nonlinear part is modeled by the Hill curve equation, presented in 3.2.

For both models, the Hill equation parameters  $C_{50}$ ,  $E_0$ ,  $E_{max}$  and  $\gamma$  are considered to be known a priori in this study. Typically, these parameters are determined during or after the surgery.

### 3.3. Control

The control schema used in this paper is presented in Fig. 3.3.

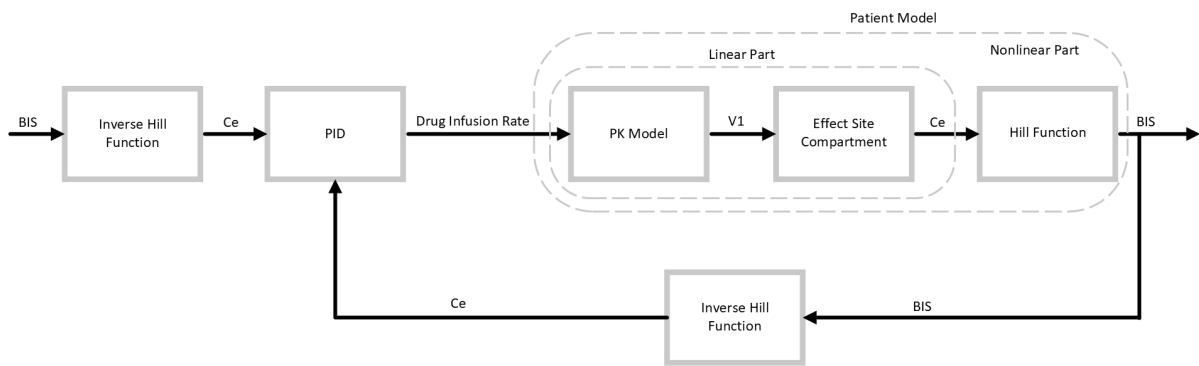


Figure 3.3: Control Scheme

First, the reference is given as a BIS value for hypnosis and as the first twitch value for neuromuscular blockade. These values need to be converted into a concentration effect values to provide the appropriate input for the controller to compute the optimal drug infusion rate that is going to be administered to the patient. At the output of the patient model, the BIS value, respectively the first twitch are measured. These measurement

are then processed through the inverse of Hill equation block to compute the equivalent concentration effect values, providing the necessary feedback to the controller.

The developed control strategies in this paper are PID, based on frequency response on Nicholis curve, an internal model control (IMC) approach, and a model-predictive control (MPC) specifically developed only for depth of anaesthesia regulation.

The PID controller minimizes the error given by the difference between the measured output and the setpoint value. It contains three parameters: proportional, integrative and derivative. The proportional term determines the ratio of the output response to the error signal, the integral term sums the error over time in order to eliminate the steady-state error, and the derivative term reacts to the rate of change of the process variable. The mathematical form of a PID controller is:

$$c(t) = K_p e(t) + K_i \int_0^t e(\tau) d\tau + K_d \frac{de(t)}{dt} \quad (3.5)$$

- $c(t)$  - control signal
- $e(t)$  - error signal
- $K_p, K_i, K_d$  - coefficients for the proportional, integrative and derivative terms

By tuning the parameters of a PID, specifically setting the optimal gains for P, I and D, we can achieve an ideal response from the control system [32].

### 3.3.1. PID Tuning with FRTool

The first PID implemented in this paper was done using FRTool (Frequency Response Tool for Computer Aided Control System Design in Matlab) which works with Nicholis diagram. This tool converts design specifications, such as overshoot, settling time and robustness, into graphical constraints, simplifying the tuning process. Graphical constraints are computed using the numerical relations for the second order systems, that can be extended for higher order systems.

In our case, the overshoot is one of the most important restrictions we must define, from which we can determine the damping factor:

$$\sigma = e^{\frac{-\pi \cdot \zeta}{\sqrt{1-\zeta^2}}} \quad (3.6)$$

The second most important constraint is the settling time, defined as:

$$t_s = \frac{2 \cdot \zeta^2 + 3}{\zeta \cdot \omega_n} \quad (3.7)$$

Once we know the settling time, the natural frequency of the equivalent second order system can be obtained.

As indicated in Equation 3.7, the need of the damping factor to determine the settling time implies that the settling time constraint can only be established once the overshoot constraint has been defined earlier.

Now, the value of the -3dB bandwidth frequency for the closed-loop can be obtained:

$$\omega_b = \omega_n \sqrt{1 - 2\zeta^2 + \sqrt{4\zeta^4 - 4\zeta^2 + 2}} \quad (3.8)$$

Robustness is another important specification for our objective, begin defined as the minimal requirement the control system has to satisfy in order to be useful in a practical environment. This is a specification related to the Nyquist plot, representing the radius of the unity circle ( $0 < R_o < 1$ ). For converting this value from the Nyquist plot to the Nicholis plot, we need the following relations:

$$\begin{cases} Re = -1 + R_o * \cos(\omega) \\ Im = R_o * \sin(\omega) \\ M_{dB} = 20 \log(\sqrt{Re^2 + Im^2}) \\ \phi_{deg} = -180 + \arctan\left(\frac{Im}{Re}\right) \cdot \frac{180}{\pi} \end{cases} \quad (3.9)$$

where  $\omega$  represents the angle of  $R_o$ .

After importing the model's transfer function into the FRTool and defining the design specifications, the interface will appear as in Figure 3.4.

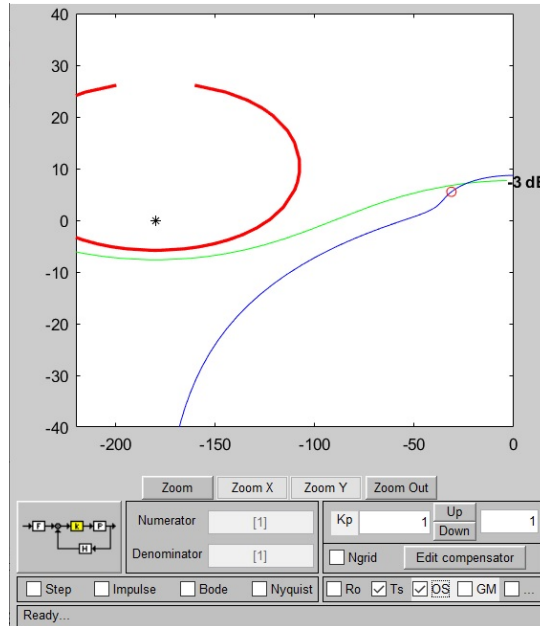


Figure 3.4: FRTool interface before designing the controller

The design specifications are met if the Nicholis curve does not intersect the overshoot constraint and if the bandwidth frequency is above the -3dB green line.

### 3.3.2. Internal Model Control Tuning

The IMC algorithm presented below is based on the lecture from [33].

The IMC (Internal Model Control) principle is based on the acknowledging that, in reality, we have an approximation of the actual process, requiring us to consider an imperfect model in the controller design. The IMC design process includes three main steps, detailed below:

#### 1. Disturbance Compensation:

The first step involves compensating for disturbances by comparing the actual output of the process with the output of the process model. In order to achieve this, the controller transfer function is written as the inverse of the plant's transfer function. If the plant transfer function is denoted by  $P(s) = \frac{A(s)}{B(s)}$ , then the controller's transfer function will be  $C(s) = \frac{B(s)}{A(s)}$ . In Figure 3.5, the initial diagram block in designing an IMC can be observed.

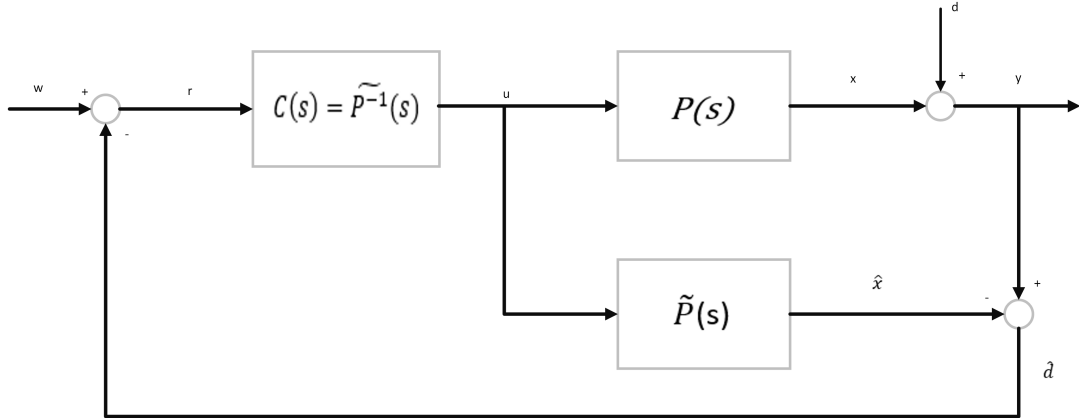


Figure 3.5: Disturbance estimation and compensation diagram block

## 2. Making the controller's transfer function proper:

If the controller's transfer function is non-proper (i.e. the degree of the numerator is greater than the degree of the denominator), it cannot be physically implemented. Since the process transfer function is strictly proper due to its physical nature (degree of  $A <$  degree of  $B$ ), its inverse will be improper. To address this, a low-pass filter is used to make the controller's transfer function proper. The filter forms can be:

- For step reference tracking:  $F(s) = \frac{1}{(1+\lambda s)^n}$
- For ramp reference tracking:  $F(s) = \frac{1+n\lambda s}{(1+\lambda s)^n}$   
where  $n$  is the order of the filter, chosen to ensure that the controller's transfer function is proper, and  $\lambda$  is a tuning parameter with effect on settling time.

## 3. Handling instability and dead-time:

If the system has elements in the right-half plane of the s-plane or includes time-delay, these elements need special handling because they can destabilize the system. The solution involves splitting the process into two parts:  $\tilde{P}_g(s)$ , the invertible part with stable poles and zeros, and  $\tilde{P}_b(s)$ , the non-invertible part containing the problematic elements. Then, the process transfer function is written as:

$$\tilde{P}(s) = \tilde{P}_g(s)\tilde{P}_b(s) \quad (3.10)$$

Dead-time can be approximated by using Padé approximations:

$$e^{-\tau_m s} = \frac{1 - \frac{\tau_m}{2}s}{1 + \frac{\tau_m}{2}s} \quad (3.11)$$

or Taylor series approximation:

$$e^{-\tau_m s} = 1 - \tau_m s \quad (3.12)$$

The controller is then computed by inverting only the invertible part of the process

$$C(s) = \tilde{P}_g(s)^{-1} F(s) \quad (3.13)$$

but the non-invertible part still has to be present in the output of the process

$$Y = P_b(s)F(s)W(s) + [1 - P_b(s)F(s)]D(s) \quad (3.14)$$

where  $P_b(s)$  is the Laplace transform of the noninvertible part of the process,  $F(s)$  is the Laplace transform of the low-pass filter,  $W(s)$  is the Laplace transform of the reference and  $D(s)$  is the Laplace transform of the disturbance applied to the system.

The block diagram of the equivalent IMC structure can be seen in the Figure 3.6. The final diagram block, along with the way to compute the controller and the closed-loop system, are provided below.

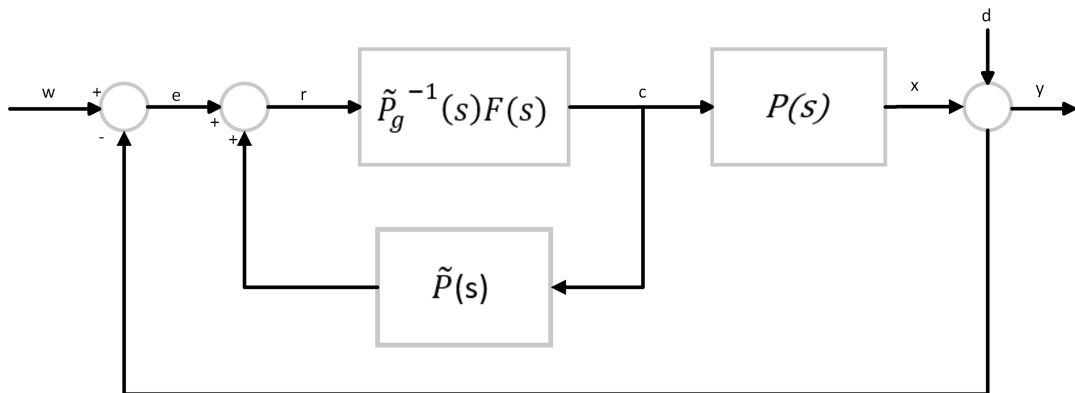


Figure 3.6: Internal Model Control Structure

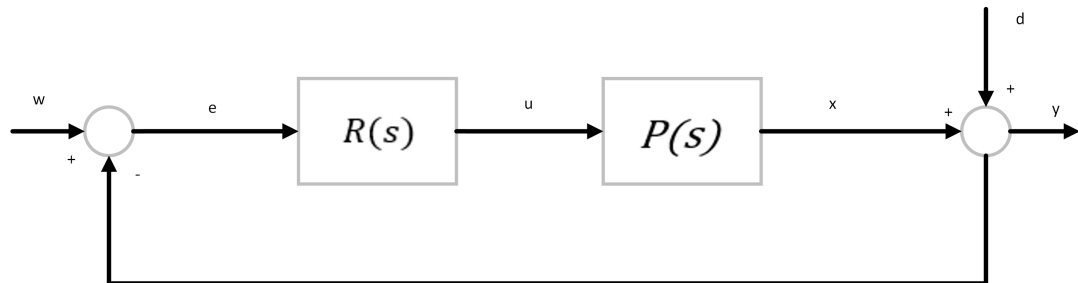


Figure 3.7: IMC final structure

$$R(s) = \frac{\tilde{P}_g^{-1}(s)F(s)}{1 - \tilde{P}_g^{-1}(s)F(s)\tilde{P}(s)} \quad (3.15)$$

$$\begin{aligned} Y(s) &= \frac{R(s)P(s)}{1 + R(s)P(s)}W(s) + \frac{1}{1 + R(s)P(s)}D(s) \\ &= \frac{\tilde{P}_g^{-1}(s)F(s)P(s)}{1 + \tilde{P}_g^{-1}(s)F(s)(P(s) - \tilde{P}(s))}W(s) + \frac{1 - \tilde{P}_g^{-1}(s)F(s)\tilde{P}(s)}{1 + \tilde{P}_g^{-1}(s)F(s)(P(s) - \tilde{P}(s))D(s)} \end{aligned} \quad (3.16)$$

### 3.3.3. Model-Predictive Control Tuning

The design of Model-Predictive Control discussed below is based on the concepts presented in the first chapter of [34].

The primary objective of model-predictive control (MPC) is to determine a future trajectory of the manipulated variable that optimizes the system's output behaviour. For that to happen, setting the prediction horizon and the control horizon are required.

Prediction horizon specifies how many future state variables will be predicted for each time step, while the control horizon indicates the extent to which future control inputs are planned to optimize the system. The visual representation of these concepts can be seen in Figure 3.8, where the MPC predicts the controlled variable and the control signal over time within the optimization window established.

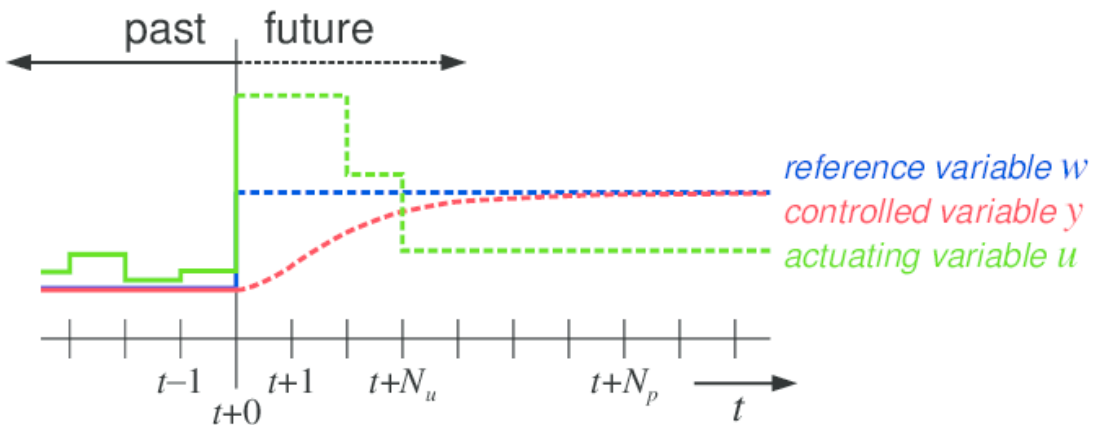


Figure 3.8: Control and prediction horizon

#### 1. Defining the system and the future control trajectory:

To design a MPC, the system needs to be written in a state-space form. For a single-input single-output (SISO) system, the state-space representation is given by:

$$\begin{cases} x_m(k+1) = A_m x_m(k) + B_m u_m(k) \\ y_m(k) = C_m x_m(k) + D_m u_m(k) \end{cases} \quad (3.17)$$

where:

- $k$  - the current sample time
- $u$  - the manipulated variable, respectively the system's input

- $y$  - the system's output
- $x_m$  - the state variable

By taking the difference operation on both sides, we obtain:

$$x_m(k+1) - x_m(k) = A_m(x_m(k) - x_m(k-1)) + B_m(u(k) - u(k-1)) \quad (3.18)$$

Defining the differences in the state and control variables by:

$$\Delta x_m(k+1) = x_m(k+1) - x_m(k) \quad (3.19)$$

$$\Delta u(k) = u(k) - u(k-1) \quad (3.20)$$

The state-space equation becomes:

$$\Delta x_m(k+1) = A_m \Delta x_m(k) + B_m \Delta u(k) \quad (3.21)$$

To link  $\Delta x_m(k)$  to  $y(k)$ , a new state variable vector is introduced:

$$x(k) = [\Delta x_m(k)^T \ y(k)]^T \quad (3.22)$$

And the output equation becomes:

$$\begin{aligned} y(k+1) - y(k) &= C_m(x_m(k+1) - x_m(k)) \\ &= C_m \Delta x_m(k+1) \\ &= C_m A_m \Delta x_m(k) + C_m B_m \Delta u(k) \end{aligned} \quad (3.23)$$

Thus, the augmented state-space model, formed by the triplet  $(A, B, C)$  will be used in control designed and is defined by:

$$\begin{aligned} \overbrace{\begin{bmatrix} \Delta x_m(k+1) \\ y(k+1) \end{bmatrix}}^{x(k+1)} &= \underbrace{\begin{bmatrix} A_m & o_m^T \\ C_m A_m & 1 \end{bmatrix}}_A \overbrace{\begin{bmatrix} \Delta x_m(k) \\ y(k) \end{bmatrix}}^{x(k)} + \underbrace{\begin{bmatrix} B_m \\ C_m B_m \end{bmatrix}}_B \Delta u(k) \\ y(k) &= \underbrace{\begin{bmatrix} o_m & 1 \end{bmatrix}}_C \begin{bmatrix} \Delta x_m(k) \\ y(k) \end{bmatrix} \end{aligned} \quad (3.24)$$

The future control trajectory is defined as:

$$\Delta u(k_i), \Delta u(k_i + 1), \dots, \Delta u(k_i + N_c - 1) \quad (3.25)$$

where  $N_c$  is the control horizon. The future state variables are:

$$x(k_i + 1|k_i), x(k_i + 2|k_i), \dots, x(k_i + N_p|k_i) \quad (3.26)$$

where  $N_p$  is the prediction horizon, and  $x(k_i + m|k_i)$  represent the predicted state variable at  $k_i + m$  with the current system information  $x(k_i)$ . The control horizon is usually chosen to be less than the prediction horizon  $N_p$ .

Using the augmented state-space model, the future state variables are computed as:

$$\begin{aligned}
 x(k_i + 1 | k_i) &= Ax(k_i) + B\Delta u(k_i) \\
 x(k_i + 2 | k_i) &= Ax(k_i + 1 | k_i) + B\Delta u(k_i + 1) \\
 &= A^2x(k_i) + AB\Delta u(k_i) + B\Delta u(k_i + 1) \\
 &\vdots \\
 x(k_i + N_p | k_i) &= A^{N_p}x(k_i) + A^{N_p-1}B\Delta u(k_i) + A^{N_p-2}B\Delta u(k_i + 1) \\
 &\quad + \cdots + A^{N_p-N_c}B\Delta u(k_i + N_c - 1)
 \end{aligned} \tag{3.27}$$

From this, predicted output variables are obtained:

$$\begin{aligned}
 y(k_i + 1 | k_i) &= CAx(k_i) + CB\Delta u(k_i) \\
 y(k_i + 2 | k_i) &= CA^2x(k_i) + CAB\Delta u(k_i) + CB\Delta u(k_i + 1) \\
 y(k_i + 3 | k_i) &= CA^3x(k_i) + CA^2B\Delta u(k_i) + CAB\Delta u(k_i + 1) + CB\Delta u(k_i + 2) \\
 &\vdots \\
 y(k_i + N_p | k_i) &= CA^{N_p}x(k_i) + CA^{N_p-1}B\Delta u(k_i) + CA^{N_p+2}B\Delta u(k_i + 1) \\
 &\quad + \cdots + CA^{N_p-N_c}B\Delta u(k_i + N_c - 1)
 \end{aligned} \tag{3.28}$$

Defining the vectors for the predicted output and future control signals:

$$Y = [y(k_i + 1 | k_i) \ y(k_i + 2 | k_i) \ \cdots \ y(k_i + N_p | k_i)]^T \tag{3.29}$$

$$\Delta U = [\Delta u(k_i) \ \Delta u(k_i + 1) \ \Delta u(k_i + 2) \ \cdots \ \Delta u(k_i + N_c - 1)]^T \tag{3.30}$$

The compact form of the predicted output becomes:

$$Y = Fx(k_i) + \Phi\Delta U \tag{3.31}$$

where

$$F = \begin{bmatrix} CA \\ CA^2 \\ CA^3 \\ \vdots \\ CA^{N_p} \end{bmatrix}; \Phi = \begin{bmatrix} CB & 0 & 0 & \cdots & 0 \\ CAB & CB & 0 & \cdots & 0 \\ CA^2B & CAB & CB & \cdots & 0 \\ \cdots & \cdots & \cdots & \cdots & \cdots \\ CA^{N_p-1}B & CA^{N_p-2}B & CA^{N_p-3}B & \cdots & CA^{N_p-N_c}B \end{bmatrix}$$

## 2. Optimization and cost function:

Given a set-point signal  $r(k_i)$ , the control system aims to bring the predicted output as close as possible to the set-point, assuming that the set-point signal remains constant within the optimization window.

The set-point vector is:

$$R_s^T = \underbrace{[1 \ 1 \ \cdots \ 1]}_{N_p} r(k_i) \tag{3.32}$$

The cost function  $J$ , that holds the control objective, is defined as:

$$J = (R_s - Y)^T(R_s - Y) + \Delta U^T \bar{R} \Delta U \quad (3.33)$$

The first term minimizes the error between the predicted output and the set-point, while the second term *penalizes the magnitude of control input changes*. To find the optimal  $\Delta U$  that minimizes  $J$ , we express  $J$  as:

$$J = (R_s - Fx(k_i))^T(R_s - Fx(k_i)) - 2\Delta U^T \Phi^T(R_s - Fx(k_i)) + \Delta U^T(\Phi^T \Phi + \bar{R})\Delta U \quad (3.34)$$

The necessary condition for minimizing  $J$  is  $\frac{\partial J}{\partial \Delta U} = 0$ , where:

$$\frac{\partial J}{\partial \Delta U} = -2\Phi^T(R_s - Fx(k_i)) + 2(\Phi^T \Phi + \bar{R})\Delta U \quad (3.35)$$

Solving for  $\Delta U$ :

$$\Delta U = (\Phi^T \Phi + \bar{R})^{-1} \Phi^T(R_s - Fx(k_i)) \quad (3.36)$$

The matrix  $(\Phi^T \Phi + \bar{R})^{-1}$  is called the Hessian matrix.  $R_s$  is a data vector containing set-point information and is expressed as:

$$R_s = \overbrace{[1 \ 1 \ 1 \ \cdots \ 1]}^{N_p} r(k_i) = \bar{R}_s r(k_i) \quad (3.37)$$

Therefore, the optimal control signal is related to the set-point signal  $r(k_i)$  and the state variable  $x(k_i)$  via:

$$\Delta U = (\Phi^T \Phi + \bar{R})^{-1} \Phi^T(\bar{R}_s r(k_i) - Fx(k_i)) \quad (3.38)$$

## Chapter 4. Detailed Design, Implementation and Results

The implementation and simulation were performed using Matlab and Simulink, two powerful tools provided by MathWorks. Matlab is a programming and numeric computing platform widely used by engineers and scientists for algorithm development, model creation and data analysis. It offers various toolboxes specialised for different fields, such as mechanical engineering, civil engineering, aerospace, biomedical processing, robotics, economics, and control systems. One of the most commonly used add-ons within Matlab is Simulink, a graphical environment for modelling, simulating and analyzing systems. It offers the possibility to observe and validate system behaviour, allowing to identify potential issues and optimize performance before deployment in real-world applications.

In both hypnosis and neuromuscular blockade scenarios, a single-input single-output (SISO) approach is used. For hypnosis, the input is propofol, and the output is the BIS measurement. In the case of neuromuscular blockade, the input is atracurium, and the output is the amplitude of the first twitch response to stimulation.

### 4.1. Hypnosis Implementation

For developing the model, patient data was taken from [35], as it can be seen in Table 4.1.

Table 4.1: Hypnosis Patients

Id	Age	Height	Weight	Gender	C50	E0	Emax	$\gamma$
1	40	163	54	1	6.33	98.8	94.1	2.24
2	36	163	50	1	6.76	98.6	86	4.29
3	28	164	52	1	8.44	91.2	80.7	4.1
4	50	163	83	1	6.44	95.9	102	2.18
5	28	164	60	2	4.93	94.7	85.3	2.46
6	43	163	59	1	12.0	90.2	147	2.42
7	37	187	75	2	8.02	92.0	104	2.1
8	38	174	80	1	6.56	95.5	76.4	4.12
9	41	170	70	1	6.15	89.2	63.8	6.89
10	37	167	58	1	13.7	83.1	151	1.65
11	42	179	78	2	4.82	91.8	77.9	1.85
12	34	172	58	1	4.95	96.2	90.8	1.84
13	38	169	65	1	7.42	93.1	96.6	3

The patients model were developed using a function script to keep organized and clean code.

First, the parameters from the pharmacokinetic model 3.1 need to be computed. Various models for propofol with similar structures have been widely developed, but they present differences in covariates and scaling of volumes and/or clearance relationships to these covariates, according to [36]. Among these models, Kataria, Short, Schuttler and Eleveld can be enumerated. However, this paper uses Schnider parameters, which are described by the following set of equations:

$$\begin{aligned}
 V_1 &= 4.27 \text{ [L]} \\
 V_2 &= 18.9 + (-0.391 \times (\text{Age} - 53)) \text{ [L]} \\
 V_3 &= 238 \text{ [L]} \\
 CL_1 &= 1.89 + 0.0456 \times (TBM - 77) - 0.0681 \times (LBM - 59) \\
 &\quad + 0.0264 \times (HT - 177) \text{ [L/min}^{-1}\text{]} \\
 CL_2 &= 1.29 - 0.024 \times (\text{Age} - 53) \text{ [L/min}^{-1}\text{]} \\
 CL_3 &= 0.836 \text{ [L/min}^{-1}\text{]} \\
 k_{10} &= \frac{CL_1}{V_1} \text{ [min}^{-1}\text{]} \\
 k_{12} &= \frac{CL_2}{V_1} \text{ [min}^{-1}\text{]} \\
 k_{13} &= \frac{CL_3}{V_1} \text{ [min}^{-1}\text{]} \\
 k_{21} &= \frac{CL_2}{V_2} \text{ [min}^{-1}\text{]} \\
 k_{31} &= \frac{CL_3}{V_3} \text{ [min}^{-1}\text{]} \\
 k_{e0} &= 0.456 \text{ [min}^{-1}\text{]} \\
 k_{1e} &= k_{e0} \text{ [min}^{-1}\text{]}
 \end{aligned} \tag{4.1}$$

where:

- $V_1$  - Volume of drug distribution in central compartment
- $V_2, V_3$  - Volume of drug distribution in peripheral compartments
- $CL_i, i = 1:3$  - Clearance (rate at which the substance is removed from the body)
- $TBM$  - Total body weight
- $HT$  - Height
- $LBM$  - Lean body mass

Values for  $TBM$  and  $HT$  can be found in Table 4.1.  $LBM$  is computed based on the patient's gender as follows:

- If the patient is a male:

$$LBM = 1.1 \cdot TBM - 128 \cdot \frac{TBM^2}{HT^2} \tag{4.2}$$

- If the patient is a female:

$$LBM = 1.07 \cdot TBM - 148 \cdot \frac{TBM^2}{HT^2} \quad (4.3)$$

(4.4)

One advantage of Schnider model is its ability to adjust the infusion rate based on the patient's age, resulting in smaller dosage administration by the pump for older patients. However, a disadvantage is that the computation of  $k_{10}$  relies on the lean body equation which can cause excessive increases in maintenance infusion rates in obese patients [36].

After obtaining the parameters, the PK and PD models can be written in the following from:

$$A_k = \begin{bmatrix} -(k_{10} + k_{12} + k_{13}) & k_{21} & k_{31} \\ k_{12} & -k_{21} & 0 \\ k_{13} & 0 & -k_{31} \end{bmatrix}, \quad B_k = \begin{bmatrix} 1 \\ 0 \\ 0 \end{bmatrix}, \quad C_k = [1 \ 0 \ 0], \quad D_k = [0]$$

$$A_d = -k_{e0}, B_d = k_{1e}, C_d = 1, D_d = 0$$

The overall model was implemented by a state-space, with the quadruplet of matrices (A, B, C, D) like:

$$A = \begin{bmatrix} -(k_{10} + k_{12} + k_{13}) & k_{21} & k_{31} & 0 \\ k_{12} & -k_{21} & 0 & 0 \\ k_{13} & 0 & -k_{31} & 0 \\ k_{41} & 0 & 0 & -k_{e0} \end{bmatrix}, \quad B = \begin{bmatrix} 1 \\ 0 \\ 0 \\ 0 \end{bmatrix}, \quad C = [1 \ 0 \ 0 \ 0], \quad D = [0]$$

After building the models, the next step is to run an open-loop simulation to test the patients' sensitivity to the drug.

As shown in Figure 4.1, patient 8 and patient 12 are the most sensitive to the drug. For the other patients, the BIS does not reach the target of 50 but remains within the recommended range. Still, for some patients, the depth of anaesthesia is induced too fast, which rises potential harm to the body's organ system. For patient 12, the BIS value drops below 40 (BIS = 37), which can lead to burst suppression associated with coma. Conversely, for patient 8, the BIS value exceeds 60 (BIS = 65), causing potential awareness during surgery, where the patient may feel the surgical procedure, but not being able to signal this problem.

In Figure 4.2, the static nonlinearity between the concentration effect  $C_e$  and the Bispectral Index  $BIS$  can be observed.  $C_e$  is the input administered by the anaesthesiologist during surgery, based on the patient's age, height, weight and gender. In the controller case, and because our model uses Schnider parameters influenced by age, the  $C_e$  value primarily depends on age. As it can be seen, for a BIS value of 50, the concentration effect varies between 5.3 and 8.7 mg mL<sup>-1</sup>.

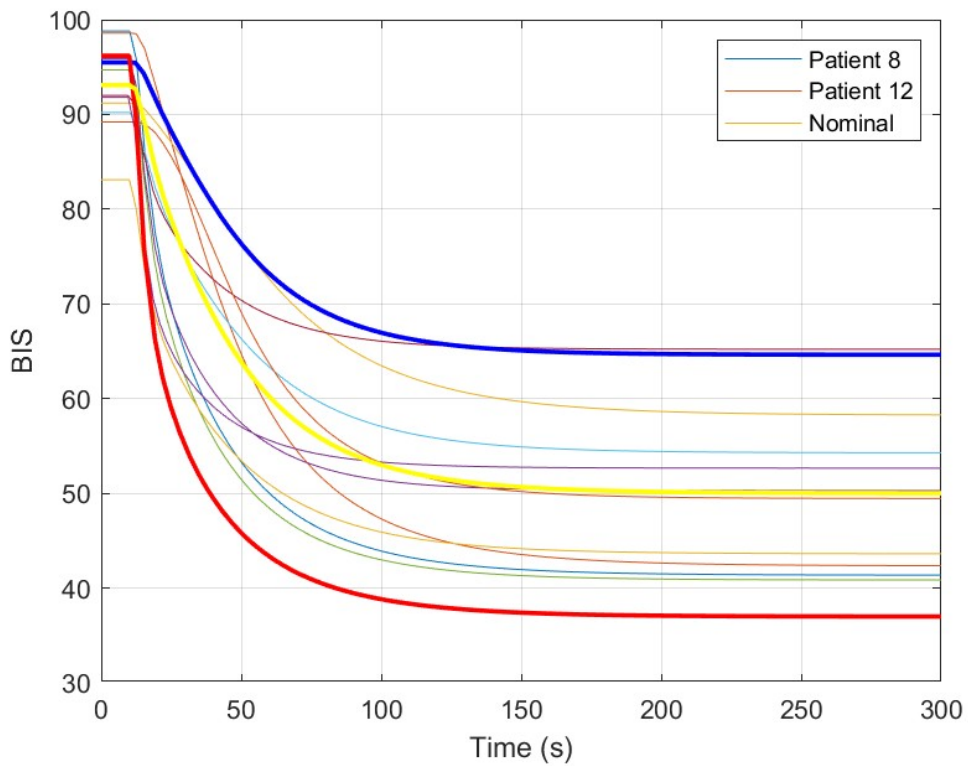


Figure 4.1: Open loop simulation

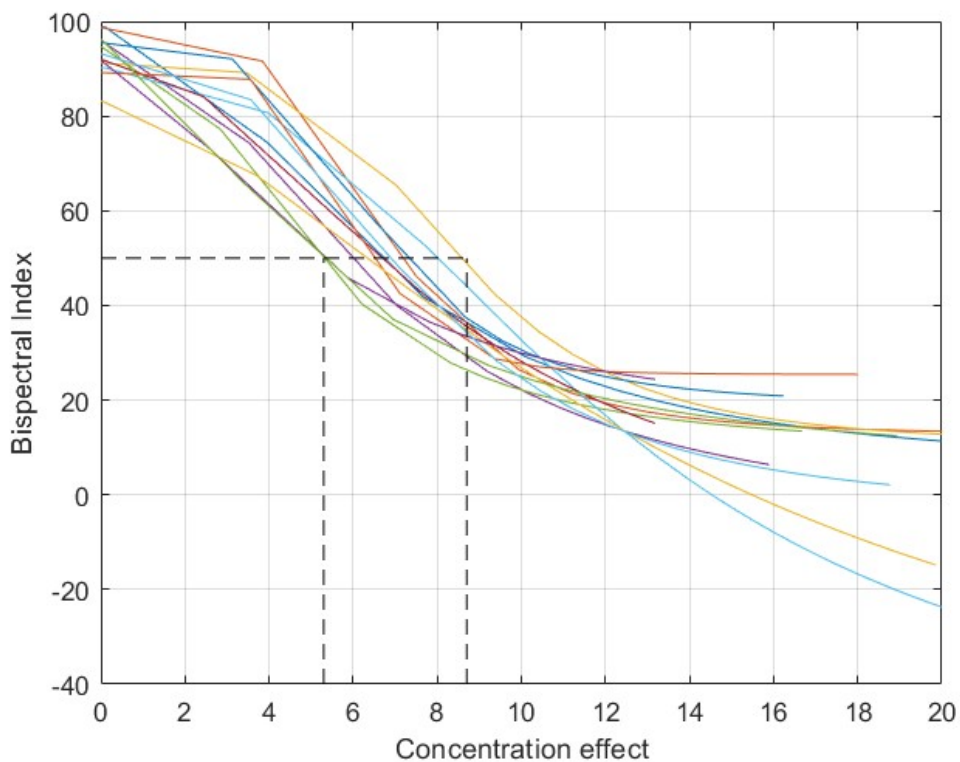


Figure 4.2: Ce vs BIS on patient model

Further, the control design process can begin. The controllers are developed based on the nominal patient's model and subsequently tested on the set of 12 patients, as listed in the Table 4.1. The control scheme presented in Figure 3.3 was implemented in Simulink using the following blocks:

- Step block: used for the BIS reference, the final value was set to 50
- Function blocks: used to implement the Hill equation and its inverse
- Transfer function blocks: used to implement the controller's and the patients' transfer functions
- Transport Delay: used to introduce a 10 seconds delay that occurs during surgery due to the measurement device

The BIS reference value of 50 is fed into the system by first passing through an inverse Hill equation block. The inverse Hill equation, presented in 3.3, converts the BIS value into a  $C_e$  value, allowing the controller to receive the appropriate input before computing the next infusion rate to be administered. After the patient receives this dose, the Hill equation block converts the  $C_e$  value back to a BIS value to verify if the patient is maintained at the correct level. The BIS measurement is then fed back to the controller in the form of a  $C_e$  value using another inverse Hill equation block.

Applying the inverse Hill equation is also known as a parameter scheduling technique [4], which linearises the system based on the compensation introduced by the Hill curve in the PD model. In the patient model, the Hill curve uses each patient's nonlinear parameters ( $E_0, E_{max}, C_{50}, \gamma$ ), whereas the inverse of Hill function uses the nominal patient's nonlinear parameters ( $E_0^{nom}, E_{max}^{nom}, C_{50}^{nom}, \gamma^{nom}$ ). The nominal patient parameters are used in compensation because these parameters are only computed during or after surgery. For this reason, these parameters will introduce errors in the nonlinearity compensation since they do not match the Hill equation parameters of each patient. This also underlines the importance of having an accurate patient model that closely reflects the reality, along with precise estimation of Hill parameters. When these conditions are met, the errors will be minimal, ensuring that the concentration effect administered by the controller will closely match the actual concentration effect needed by the patient in the real scenario to maintain the desired depth of anaesthesia.

Next, the responses for each designed controller is presented and discussed. These controllers are developed for the induction phase, which is clinically recommended to last a maximum of 4-5 minutes. During this time, the BIS value must stabilize at 50. While undershoot or overshoot may still occur, they need to be minimal to ensure the BIS remains within the range of 40-60.

#### 4.1.1. PID Controller Tuned With FR Tool

The first controller presented is designed using the FR tool. Initially, the nominal patient's transfer function was imported into the tool. The following design specifications are imposed: a settling time of 180 seconds, an overshoot of 10% to maintain BIS values within the safe range of 40-60, and a robustness of 0.7. Robustness is important as the controller will be tested on other patients as well.

To meet the specifications, the zeros were placed at  $z_1 = -0.44$  and  $z_2 = -19.68$ . This placements ensured that the Nicholis curve does not intersect the overshoot graphical constraint, and the bandwidth frequency is above the -3dB line. The resulting PID controller transfer function is:

$$H_{PID} = 0.2012(1 + 0.4324\frac{1}{s} + 0.0497s)$$

The nominal patient's response can be seen in the Figure 4.3. The BIS value reaches and maintains the set-point within 180 seconds without undershoot or overshoot.

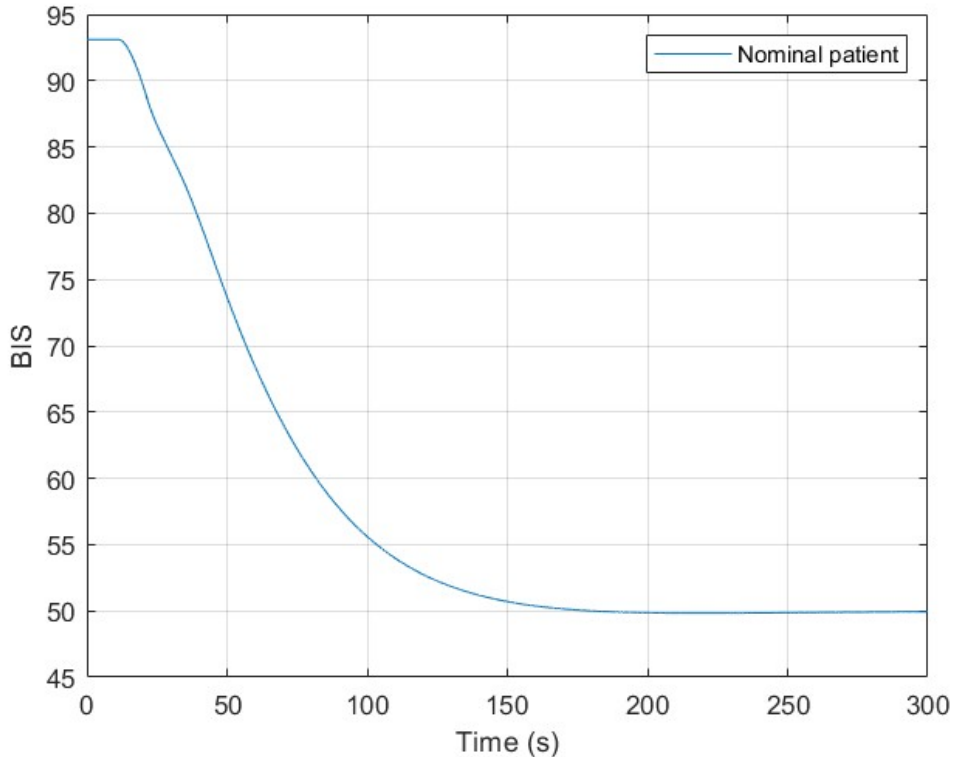


Figure 4.3: Nominal patient's response to PID designed with FR tool

However, when applying the same controller to the other patients (refer to Figure 4.4), the high intra- and inter-patient variability leads to inconsistent results. In the first 50 seconds, patients 1, 2, 4, 5, 8 and 12 experience sudden variations in the BIS value before stabilizing to the target value. Patients 7, 10 and 11 have an increased settling time, exceeding 300 seconds (5 minutes) to achieve the target. Also, patient 2 shows a minor, insignificant undershoot.

Despite these variations, the controller effectively induces and maintains the BIS within the recommended range. The highest BIS value is measured at 53 and the lowest at 48, values closer to the target than to the extremes of the range (40-60).

Regarding the control signal, specifically the drug bolus administered to each patient, Figure 4.5 shows that the controller generally administers small boluses. This is also seen in Figure 4.6, which displays all the error signals, indicating that the error approaches zero in most cases. For patients with an increased settling time, the error deviates from zero but remains very close to it. Moreover, for one patient, the administered dose exceeds the maximum value of  $8.7 \text{ mg mL}^{-1}$  obtained from the  $C_e$  versus  $BIS$  plot (see Figure 4.2).

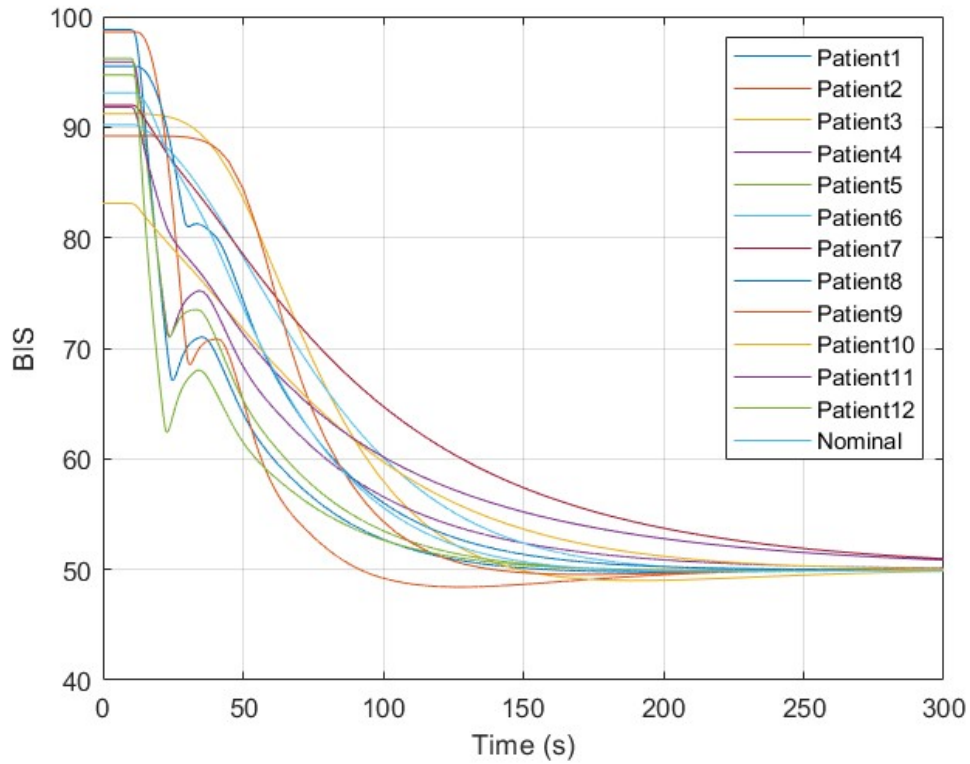


Figure 4.4: All patients response to PID designed with FR tool

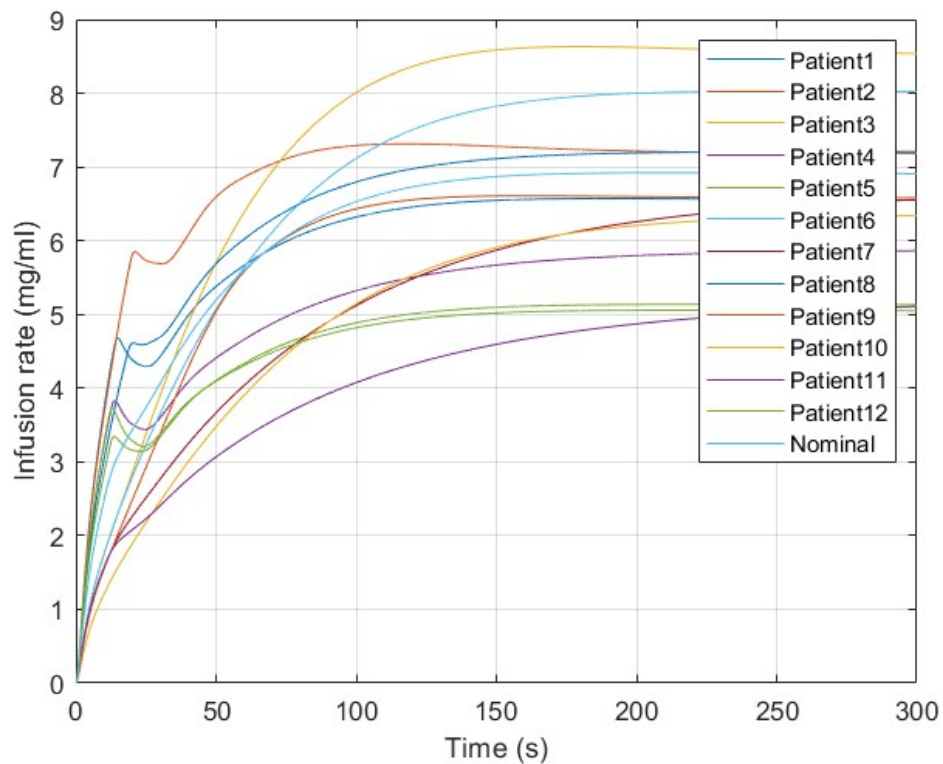


Figure 4.5: Infusion rates of PID designed with FR tool

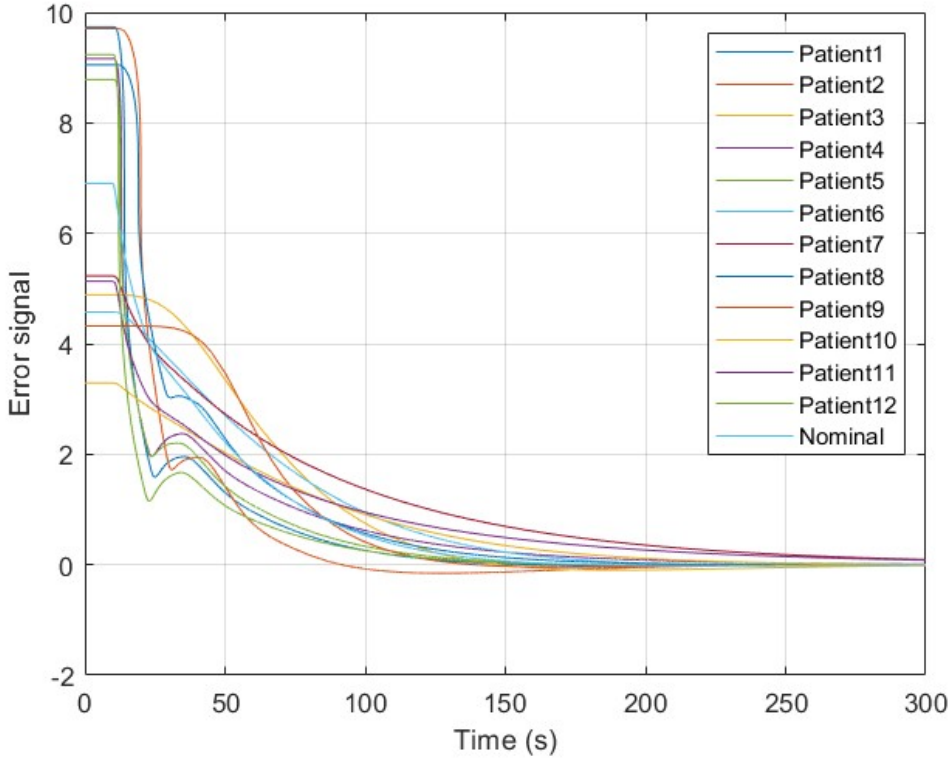


Figure 4.6: Error signal of PID designed with FR tool

#### 4.1.2. IMC Tuning

To implement the IMC, we follow the algorithm outlined in 3.3.2. The first step is to write the controller's transfer function as the inverse of the system's transfer function. For our nominal patient model, the transfer function is:

$$H_{nom}(s) = \frac{0.456(s + 0.3513)(s + 0.6663)}{(s + 1.071)(s + 0.456)(s + 0.2666)(s + 0.03014)} e^{-10s}$$

This results in the initial controller transfer function:

$$C(s) = \frac{(s + 1.071)(s + 0.456)(s + 0.2666)(s + 0.03014)}{0.456(s + 0.3513)(s + 0.6663)e^{-10s}}$$

Here,  $C(s)$  is improper, as the numerator has a higher order than the order of the denominator. To address this, we add a second-order filter to make the controller proper:

$$F(s) = \frac{1}{(\lambda s + 1)^2}$$

The value of  $\lambda$  will be chosen later in this section.

Next, we split the process into a stable part and an unstable part. The system poles are located at  $p_1 = -1.071$ ,  $p_2 = -0.456$ ,  $p_3 = -0.2666$  and  $p_4 = -0.03014$ , all in the left-half plane, indicating that the system is stable. However, the instability is introduced by the measurement device, that introduces a 10 seconds delay. This is approximated by using Taylor series approximation:

$$e^{-10s} = 1 - 10s$$

Thus, the invertible part of the system remains equal to the nominal patient's transfer function:

$$\tilde{P}_g(s) = \frac{0.456(s + 0.3513)(s + 0.6663)}{(s + 1.071)(s + 0.456)(s + 0.2666)(s + 0.03014)}$$

While the non-invertible part is the time-delay approximation:

$$\tilde{P}_b(s) = 1 - 10s$$

In Figure 3.6, the final controller is computed through block reduction, as given by the equation 3.15. After tuning, the filter parameter  $\lambda$  is set to 18, resulting in the final controller transfer function:

$$R = \frac{0.0067685(s + 1.071)(s + 0.456)(s + 0.2666)(s + 0.03014)}{s(s + 0.3513)(s + 0.142)(s + 0.06663)}$$

The controller response is shown in Figure 4.7. The settling time is 143 seconds, which is faster than the controller designed using the FR tool. Also, Figure 4.8 demonstrates that patients respond better to the IMC, with smoother responses overall. Despite this, patients 7, 10 and 11 still exhibit an increased settling time and patient 2 presents a 12% undershoot, indicating nonoptimal performance. Therefore, a compromise is made by increasing the value of  $\lambda$ . This adjustment will lead to a longer settling time for most patients, but it will reduce the undershoot to 10%, which is within the acceptable range. The results with  $\lambda = 25$  are displayed in Figure 4.9. With this new value for  $\lambda$ , the settling time for the nominal patient increases to 190 seconds (3 minutes and 10 seconds), still meeting the settling time requirement.

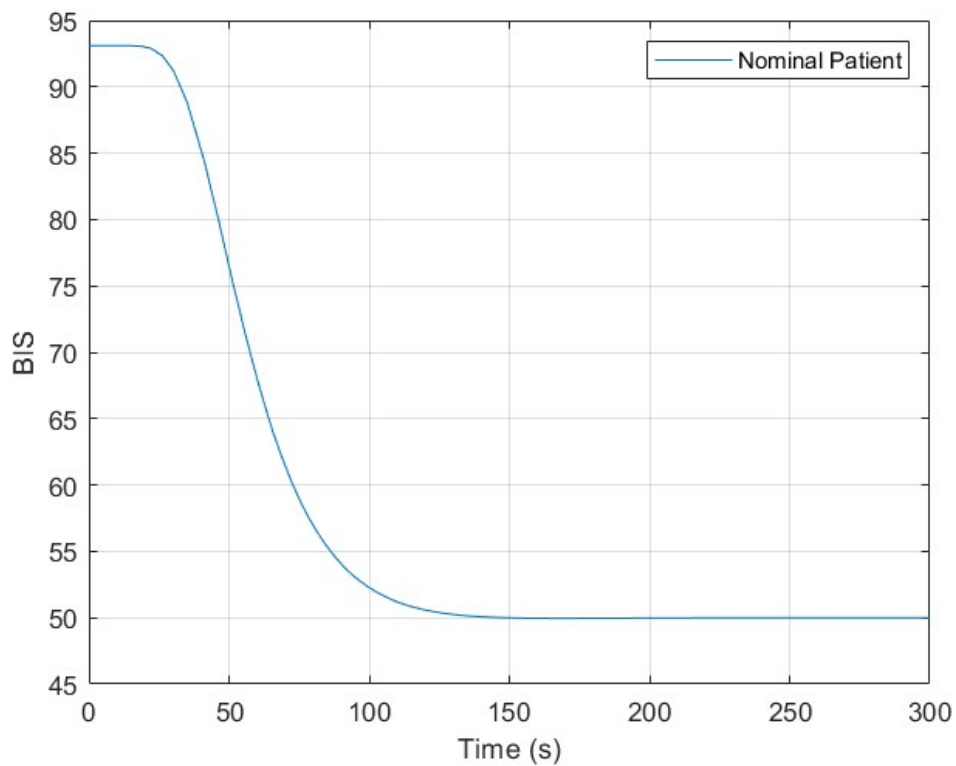
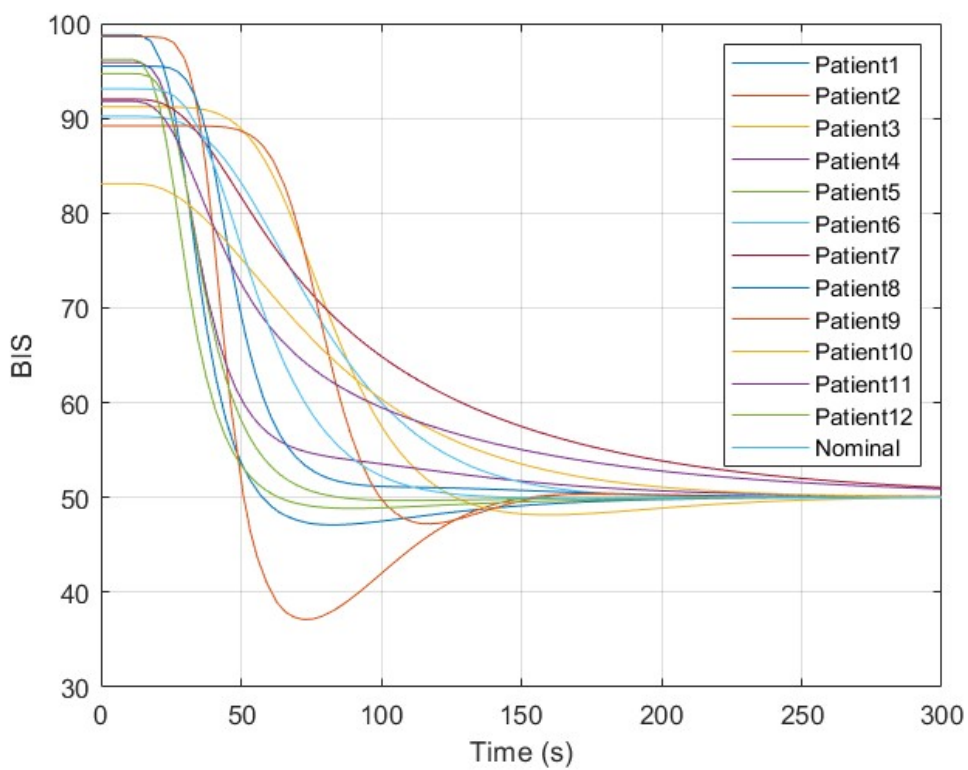


Figure 4.7: Nominal patient's response to IMC

Figure 4.8: All patients response to IMC if  $\lambda = 18$

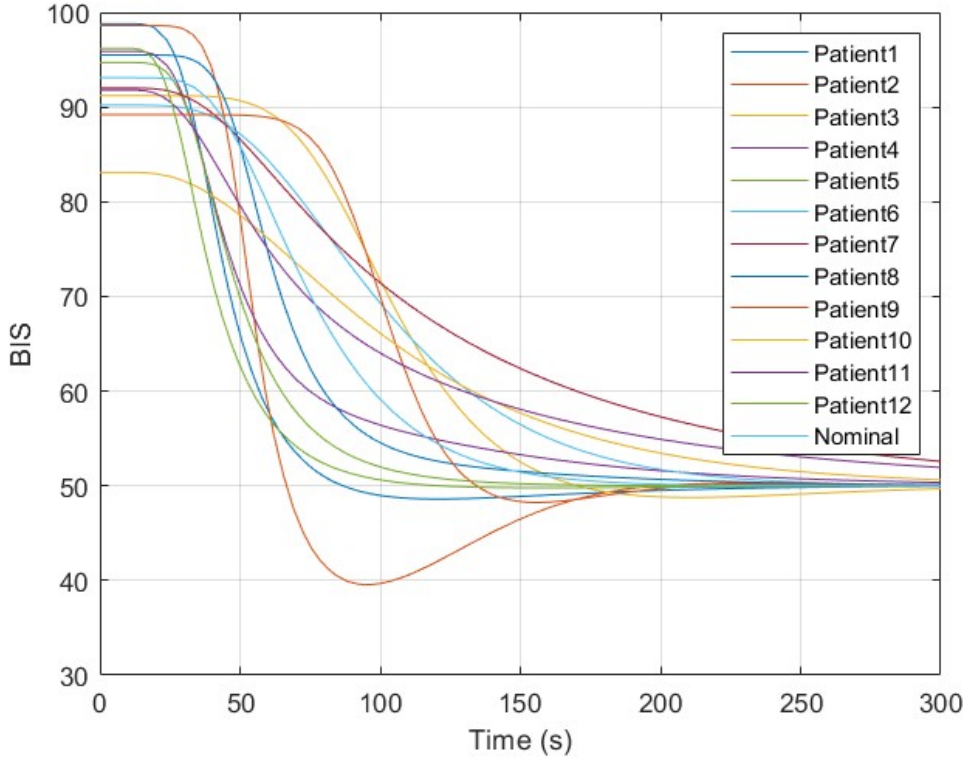


Figure 4.9: All patients response to IMC if  $\lambda = 25$

Figure 4.10 shows the control signals. Compared to the control signals from the FR controller, the drug dosages administered by the IMC are smaller, which is favourable. The highest drug dosage administered is  $3.5 \text{ mg mL}^{-1}$  for  $\lambda = 18$ , while for  $\lambda = 25$ , the highest dosage is even smaller at  $3.3 \text{ mg mL}^{-1}$ . Overall, the IMC performs better than the previous controller, as it handles intra- and inter-patient variability more effectively, resulting in smoother patient responses and lower drug dosages.

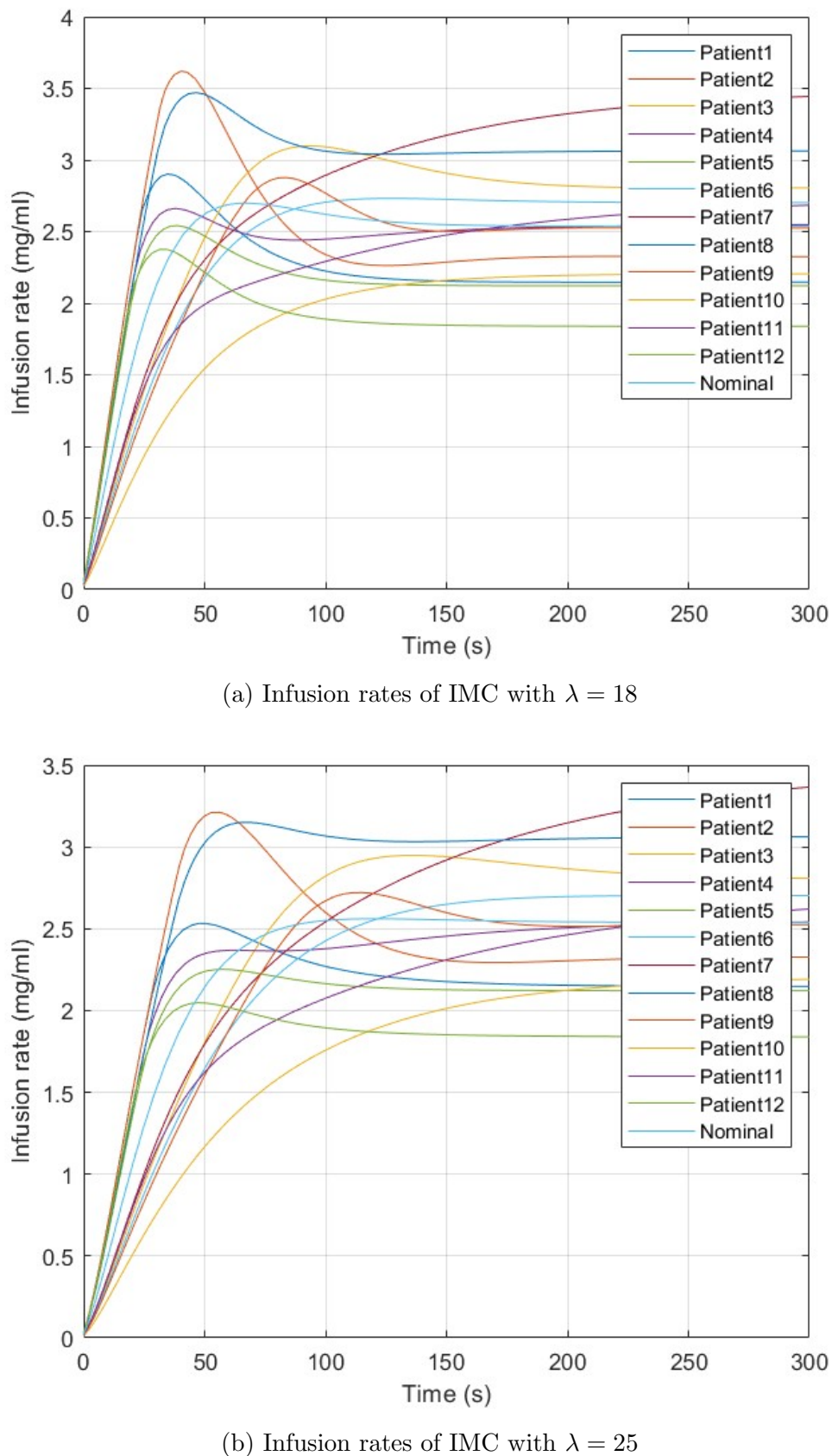
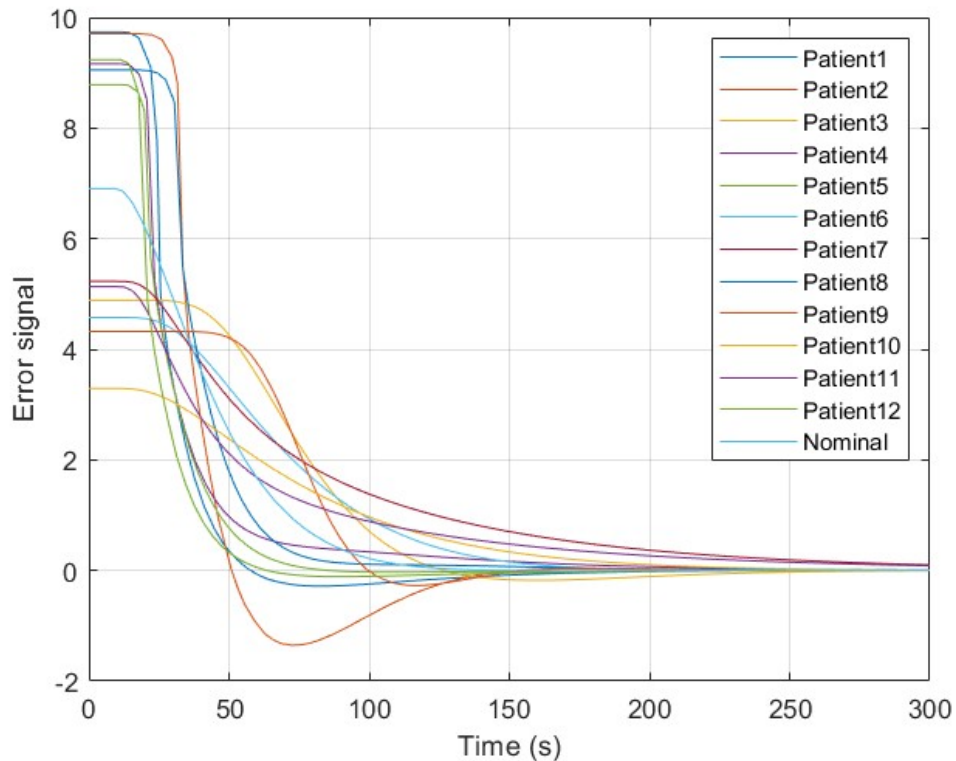
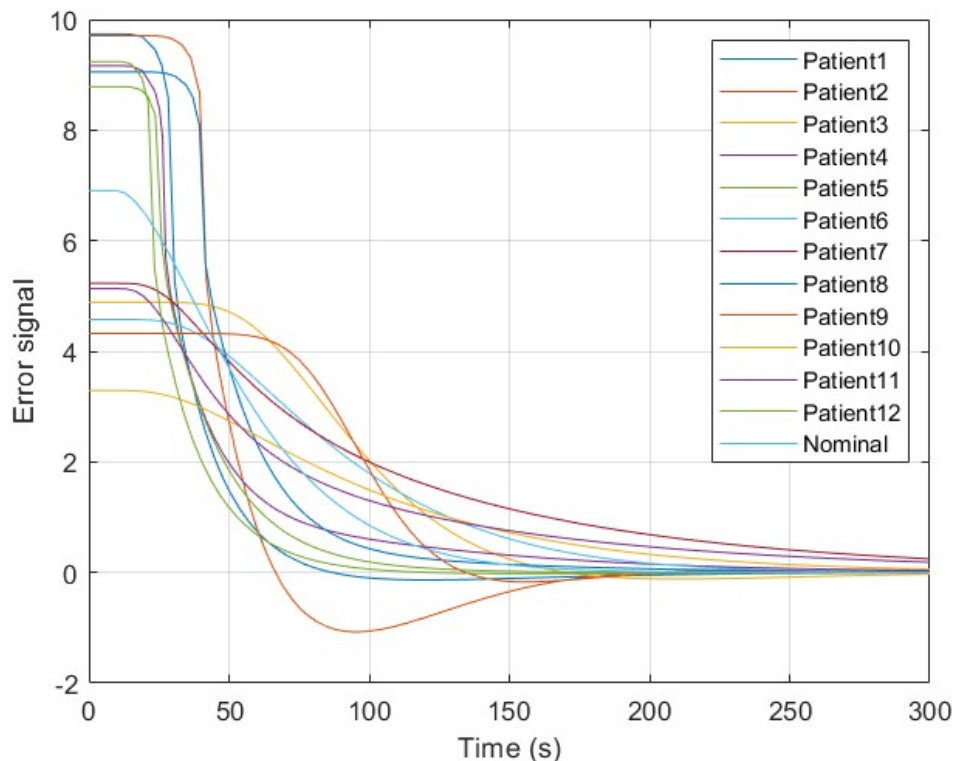


Figure 4.10: Infusion rates of the IMC controllers



(a) Error signal of IMC with  $\lambda = 18$



(b) Error signal of IMC with  $\lambda = 25$

Figure 4.11: Error signals of the IMC controllers

### 4.1.3. MPC Tuning

The next controller developed in this paper is the MPC, based on the algorithm detailed in Section 3.3.3. This controller was implemented through custom code, provided by [34]. The prediction horizon was set to  $N_p = 20$ , and the control horizon to  $N_c = 2$ . Figure 4.12 illustrates the nominal patient response, reaching the target within 90 seconds (settling time  $t_s = 90s$ ) without any fluctuations. Figure 4.13 depicts the response of all patients using the same controller. Compared to the controllers presented in the previous subsections, the MPC shows no overshoot or undershoot and has a shorter settling time, achieving the desired depth of anaesthesia more rapidly. Moreover, Figure 4.14 shows that the administered doses are stable, unlike those for the PID-IMC or PID designed with the FR tool. The highest infusion rate recorded is at  $5.1 \text{ mg mL}^{-1}$  for patient 10. Also, Figure 4.15 shows that the error is minimized quickly, within the first 100 seconds.

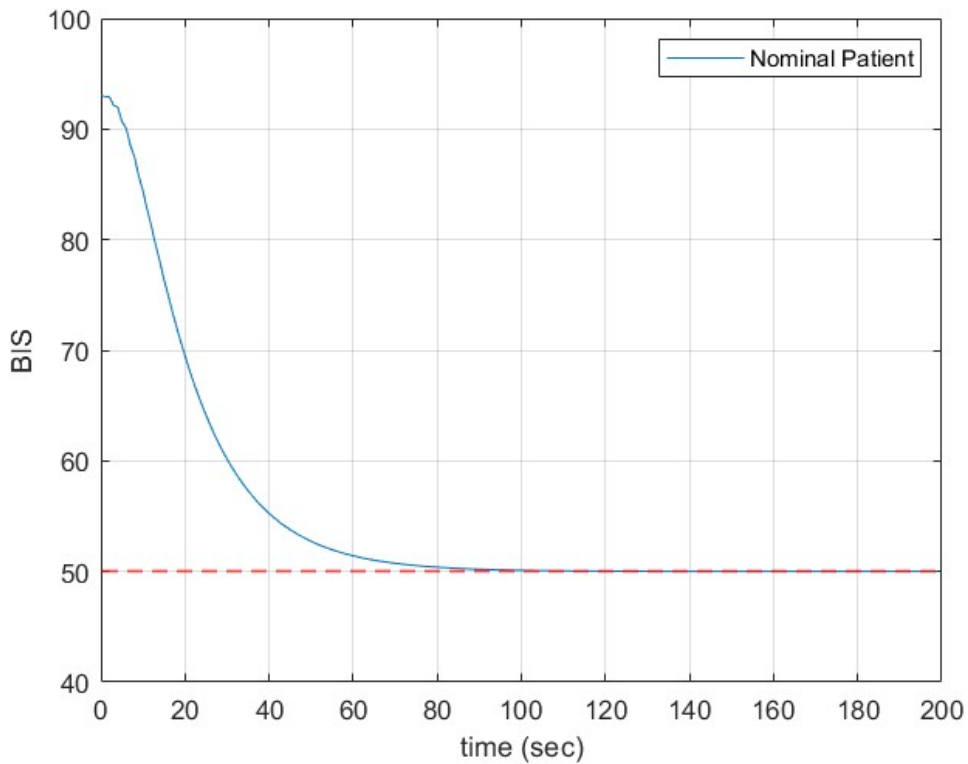


Figure 4.12: Nominal patient's response to MPC

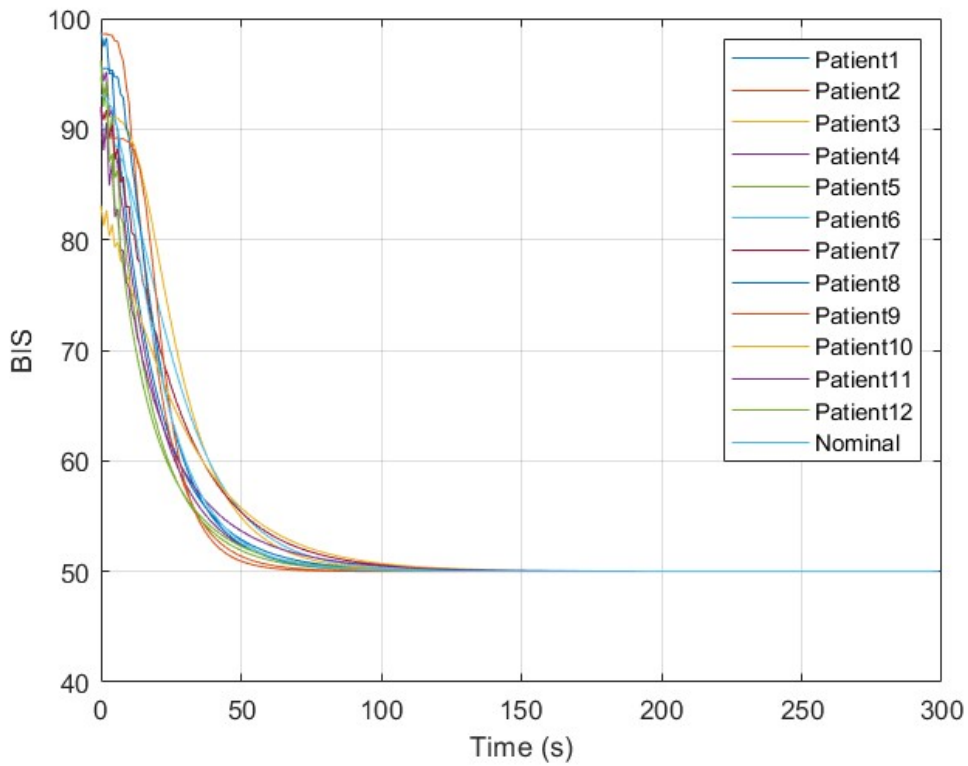


Figure 4.13: All patients response to MPC

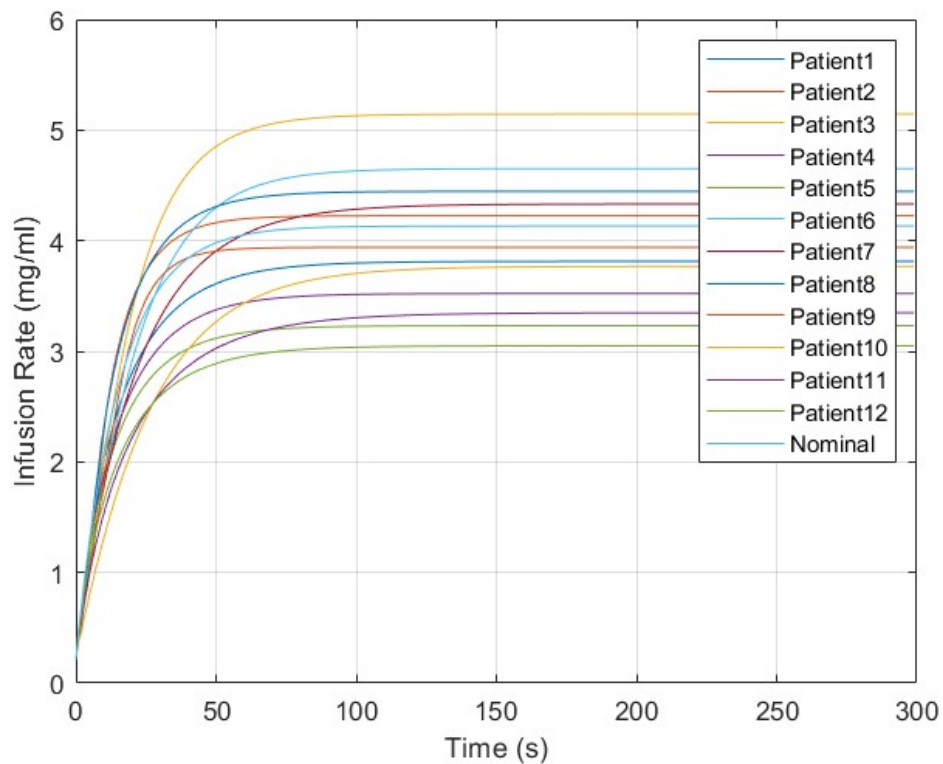


Figure 4.14: Infusion rates of MPC

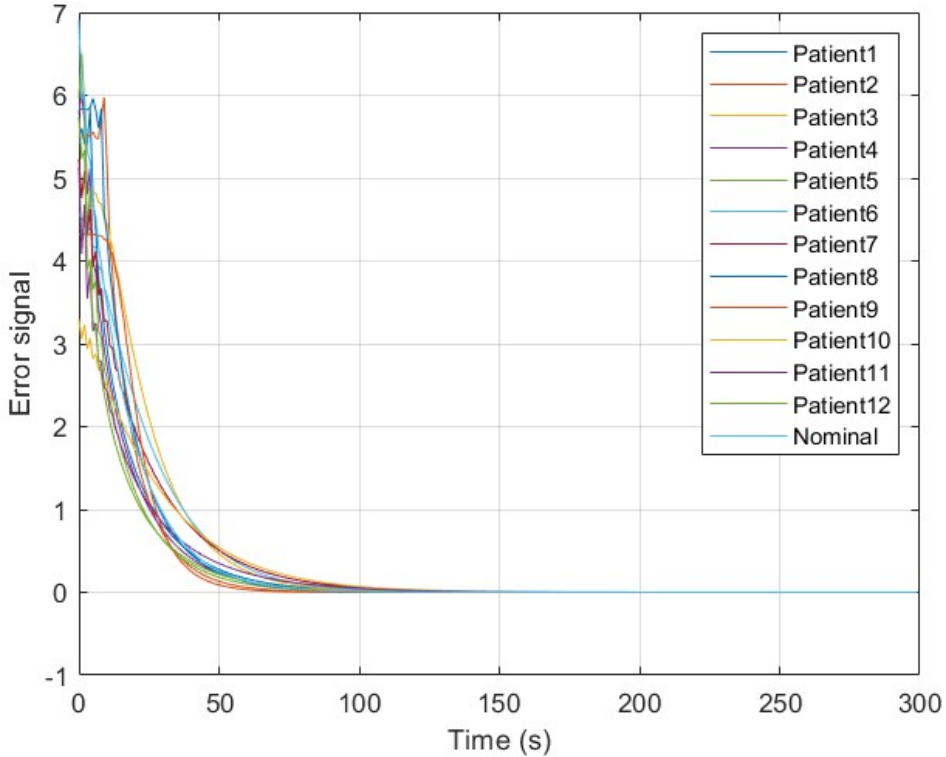


Figure 4.15: Error signals of MPC

#### 4.1.4. Controllers Response to Perturbation

To further evaluate the performance of the developed controllers, their ability to reject perturbations during surgery is tested. Although the controllers were designed for the induction phase, perturbations occur during the maintenance phase. Therefore, the simulation is extended to a simulation time of 5400 seconds (1 hour and 30 minutes). The disturbance is introduced after 10 minutes in surgery simulation, and the generated disturbance signal is shown in Figure 4.16.

Disturbance signals are unwanted inputs that disrupt the proper functioning of a system, thus increasing the error. When designing a control system, it is important to estimate potential disturbances and implement strategies to compensate for or reject them. In this study, a generated disturbance signal is used, as the one presented in [37]. It has several defined intervals: A represents the response to intubation, B represents a surgical incision, C represents a sudden stimulus following a period of low-level stimulation, D represents continuous normal stimulation, E, F, and G simulate short stimulations during surgery, and H represents stimulation during the closing phase of the surgery. It is important to observe the controller's response to this disturbance, as they should return the BIS value to the target. The disturbance was applied to the system output before measuring the BIS value.

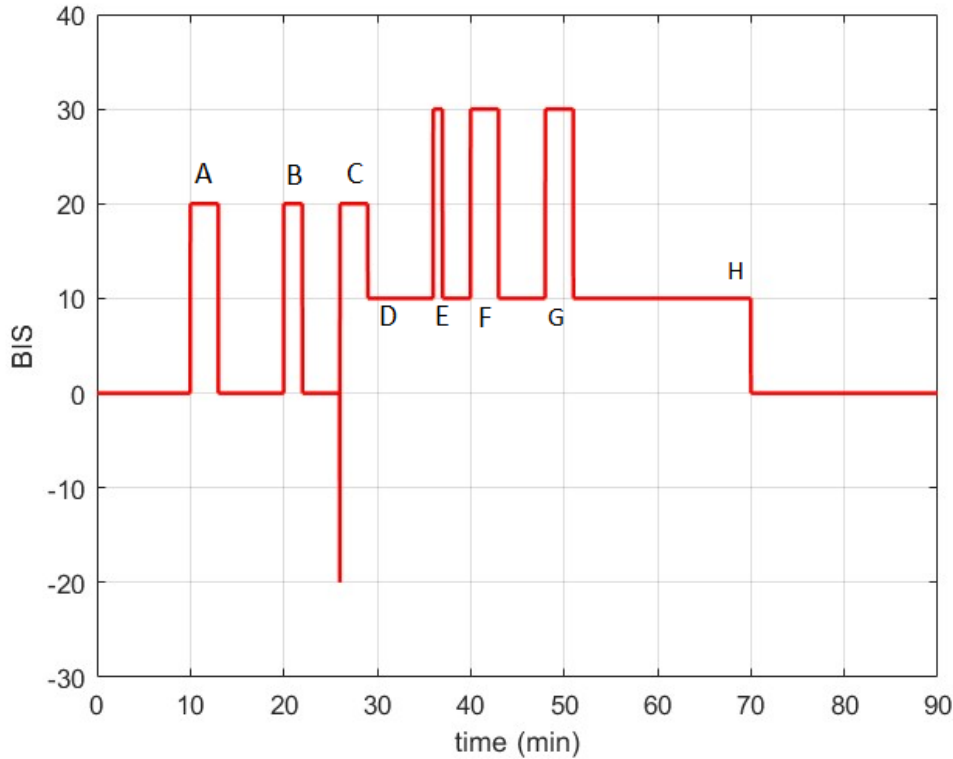


Figure 4.16: Generated disturbance signal

### 1. PID FR tool response to disturbance:

As shown in Figure 4.17, the controller maintains the BIS value within a range of 30-70 during the disturbance, exceeding the recommended range by 10 on both ends. During the C section, the BIS value briefly drops below 30. Also, the administered infusion rates increase, peaking at  $13 \text{ mg mL}^{-1}$  (Figure 4.18), resulting in a greater error deviation from zero (Figure 4.19).

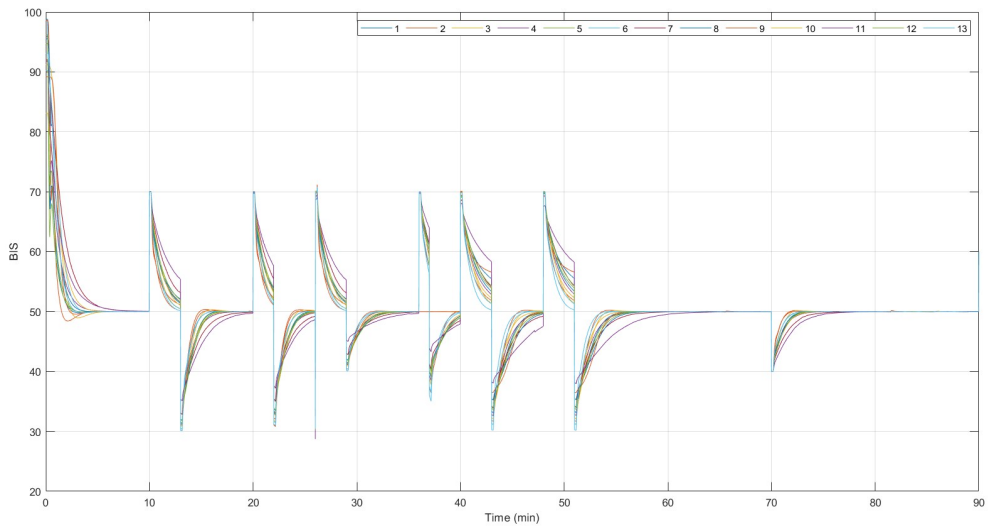


Figure 4.17: PID disturbance rejection - all patients response

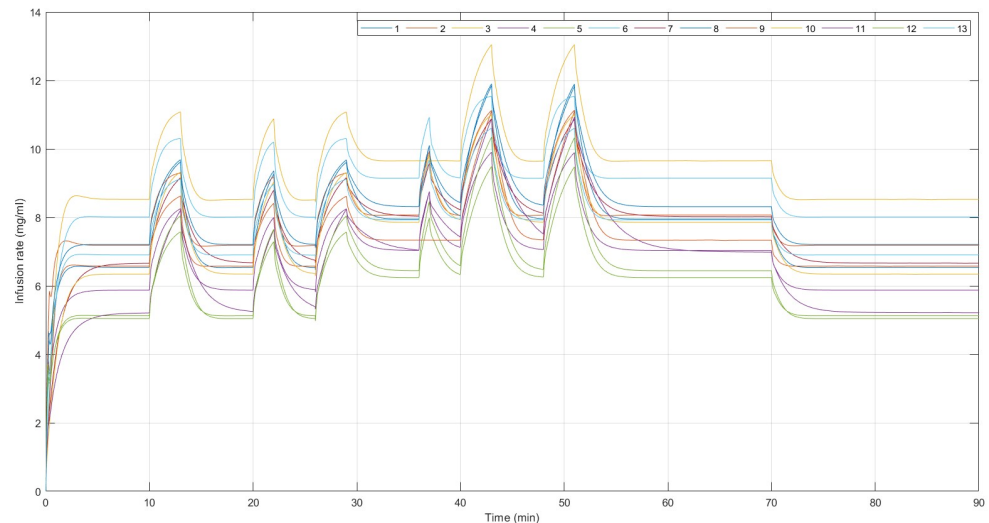


Figure 4.18: PID disturbance rejection - infusion rates

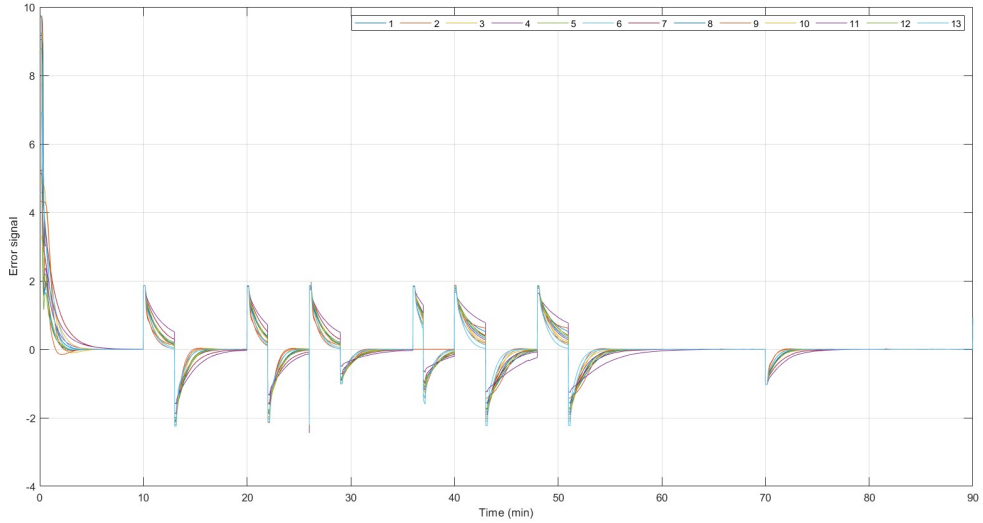


Figure 4.19: PID disturbance rejection - error signals

## 2. IMC response to disturbance:

The IMC presents similar performance in disturbance rejection as the previous controller, with the notable difference being during the C section of the disturbance, when the BIS remains above 30. The highest infusion rate recorded is  $5.8 \text{ mg mL}^{-1}$  (Figure 4.21), compared to a peak of  $3.5 \text{ mg mL}^{-1}$  in the absence of disturbance.

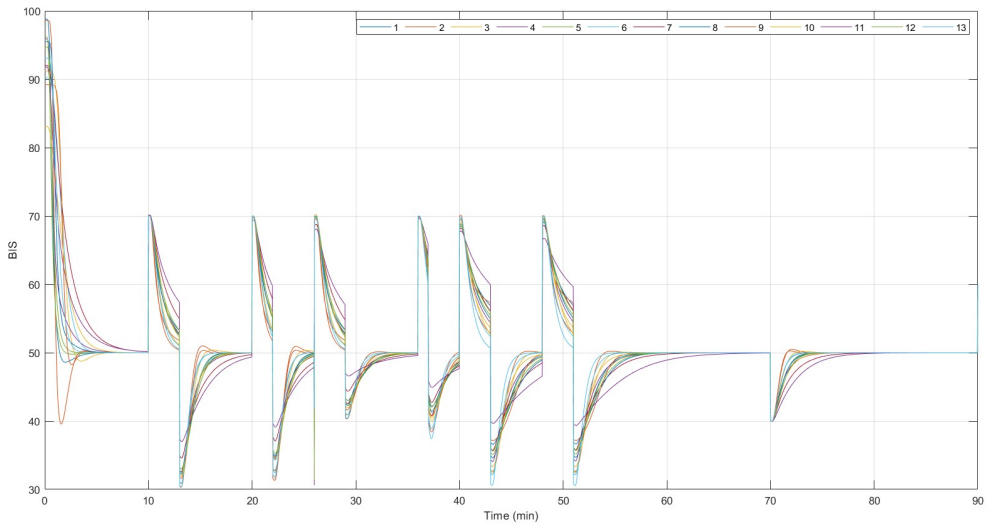


Figure 4.20: IMC disturbance rejection - all patients response

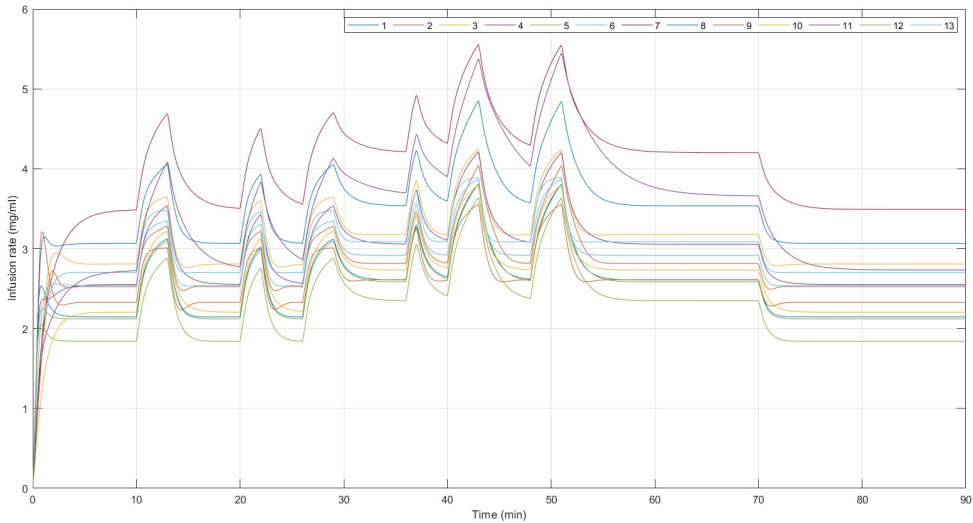


Figure 4.21: IMC disturbance rejection - infusion rates

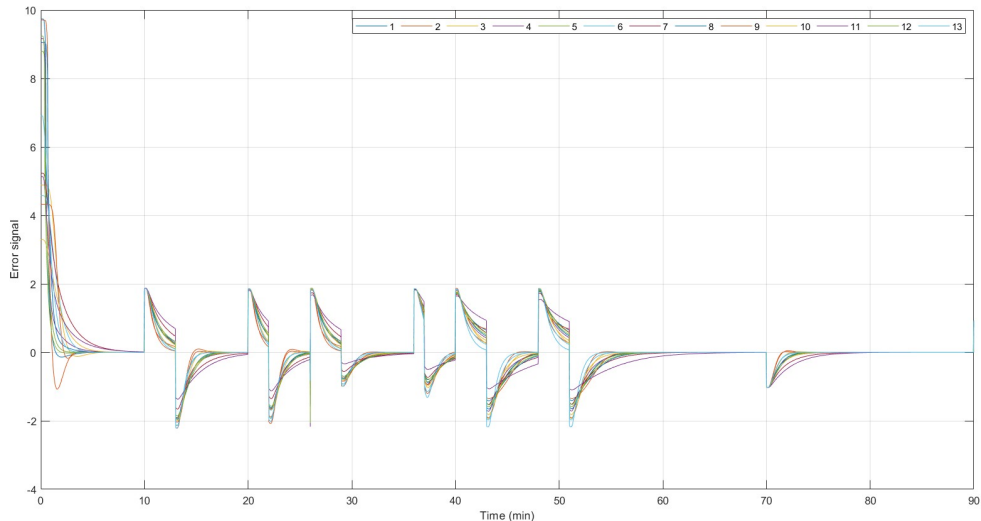


Figure 4.22: IMC disturbance rejection - error signals

### 3. MPC response to disturbance:

The MPC narrows the range of BIS fluctuations during the disturbance, keeping it between 33-70 for most of the time. However, in response to the C section, the BIS value drops below 20 and rises nearly to 90, which is highly undesirable. In the E section, the MPC performs better, bringing the BIS value closer to 40. The highest infusion rate recorded is  $7 \text{ mg mL}^{-1}$ , compared to  $5.1 \text{ mg mL}^{-1}$  without disturbance.

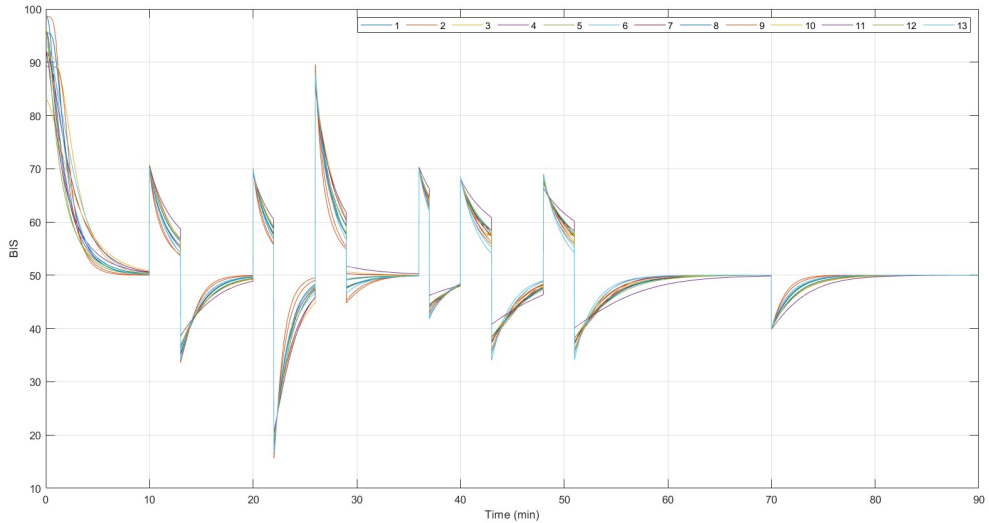


Figure 4.23: MPC disturbance rejection - all patients response

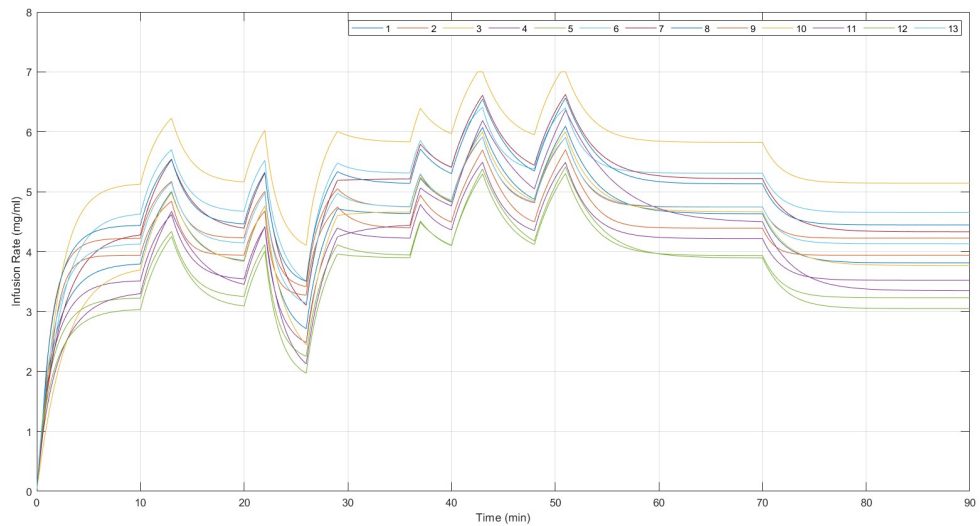


Figure 4.24: MPC disturbance rejection - infusion rates

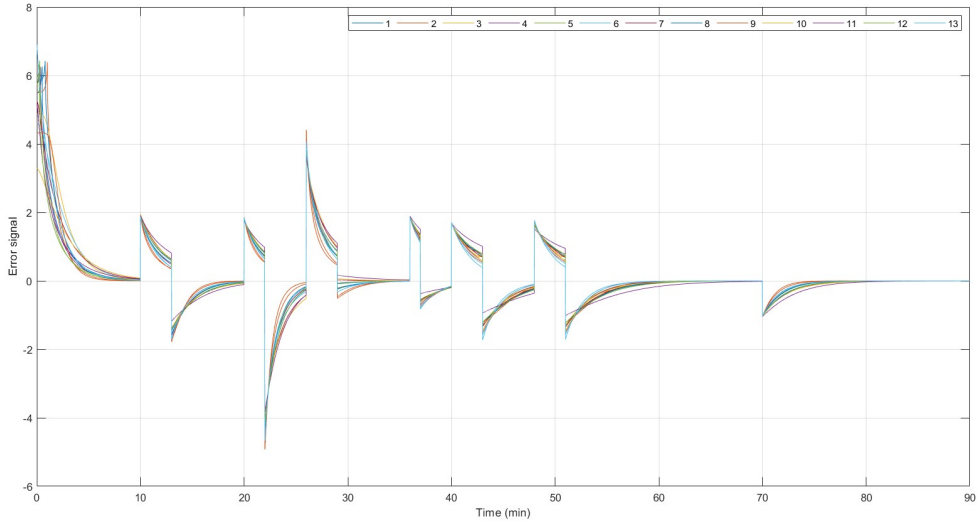


Figure 4.25: MPC disturbance rejection - error signals

## 4.2. Neuromuscular Blockade Implementation

For developing the neuromuscular blockade model and control, the patient data was taken from [30] as shown in Table 4.2

Table 4.2: Neuromuscular blockade patients - identified parameters

Id	k	p	z	$\zeta$	$\omega_n$	$\gamma$	C50
1	0.00113	0.040	0.1330	0.61	0.00134	3.10	15.1
2	0.00157	0.050	0.1336	0.86	0.00114	1.83	6.26
3	0.00150	0.045	0.1340	0.76	0.00128	2.20	7.82
4	0.00140	0.043	0.1330	0.96	0.00130	3.24	10.57
5	0.00170	0.048	0.1390	0.50	0.00230	1.60	3.00
6	0.00168	0.044	0.1340	0.50	0.00236	1.40	1.13
7	0.00222	0.049	0.1330	0.69	0.00144	2.27	7.27
8	0.00145	0.047	0.1320	0.86	0.00122	1.95	5.76
9	0.00160	0.045	0.1340	0.65	0.00160	2.19	7.11

The model used in this paper is the same as the one in [30], and it is discussed in more detail in [6]. This model is presented in equation 3.4. The same procedure used for hypnosis control is applied here: the control is developed based on the nominal patient model and then tested on a set of 8 patients to evaluate performance. The control methods developed for neuromuscular blockade are PID with FR tool and PID-IMC.

The degree of neuromuscular blockade is measured as the amplitude of the first twitch measured with the TOF device. The reference value is  $T_1 = 10\%$ , ensuring a neuromuscular block deep enough for surgery without excessively prolonging recovery [30].

An open loop simulation was first performed, as illustrated in Figure 4.26. Patient 1 and patient 6 show increased sensitivity, with patient 1 exceeding the 10% reference and patient 6 approaching 0%.

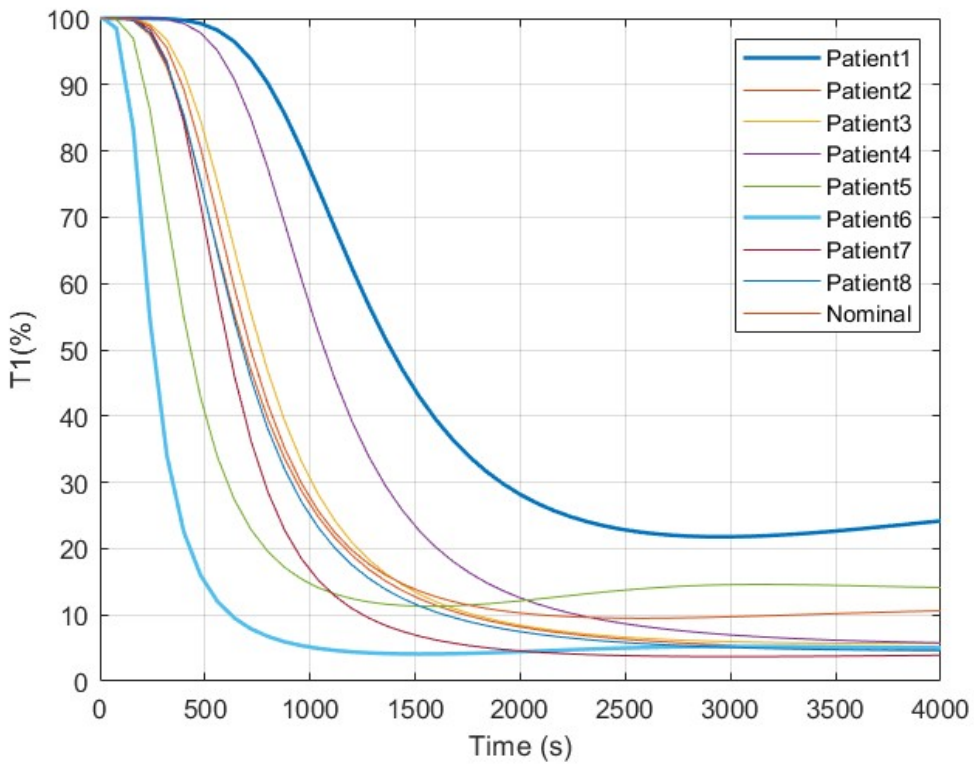


Figure 4.26: Open-loop simulation for neuromuscular blockade

The neuromuscular blockade control scheme operates similarly to the hypnosis control scheme. The pharmacodynamic model is represented by the Hill equation (equation 3.2). For this case, the parameters  $E_0$  and  $E_{max}$  were set to 100. This equation introduces a nonlinearity that is compensated through the inverse of the Hill function (equation 3.3). The parameters of the latter function are based on the nominal patient and they are estimated before surgery. The Hill equation parameters in the patient model are estimated during surgery and must be accurate to minimize errors and closely match the actual patient dynamics.

#### 4.2.1. PID Controller Tuned With FR Tool

After importing the nominal patient's transfer function into the FR tool, the following design specifications are imposed: a settling time of 60 minutes, an overshoot of 25%, and robustness of 0.7. The resulting controller introduces two zeros at  $z_1 = -0.001023$  and  $z_2 = -0.0039$  and has the following form:

$$H_{PID}(s) = 0.001428 + 1.158 \cdot 10^{-6} \frac{1}{s} + 0.29s$$

The response of the nominal patient is shown in Figure 4.27. It presents an initial undershoot but stabilizes after 25 minutes. The responses of other patients are similar

(see Figure 4.27), except for Patient 6, who exhibits a minor overshoot between minutes 20 and 43 before stabilizing at the target.

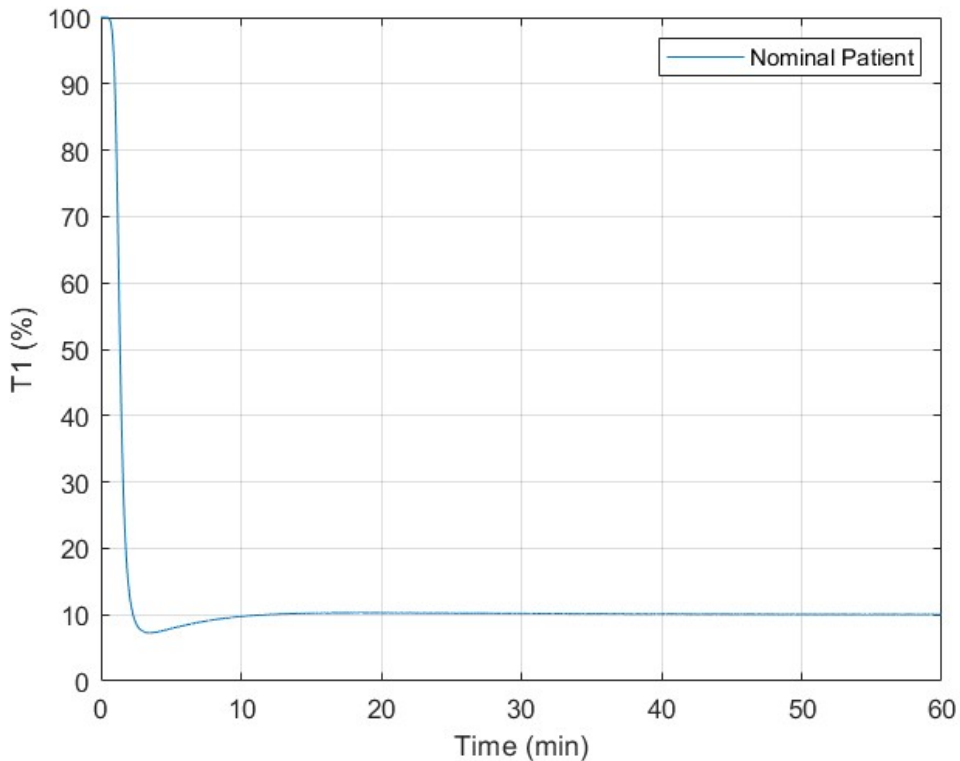


Figure 4.27: Nominal patient's response to PID designed with FR tool

Figure 4.29 shows the drug administration rate for each patient, with the plot zoomed in due to oscillations around 0, mainly between -0.01 and 0.01 mg/sec. Figure 4.30 shows that the controller minimizes the error for all patients within 30 minutes, except for Patient 6, who has an increased settling time of 50 minutes due to an overshoot in the response, but it still meets the settling time constraint imposed.

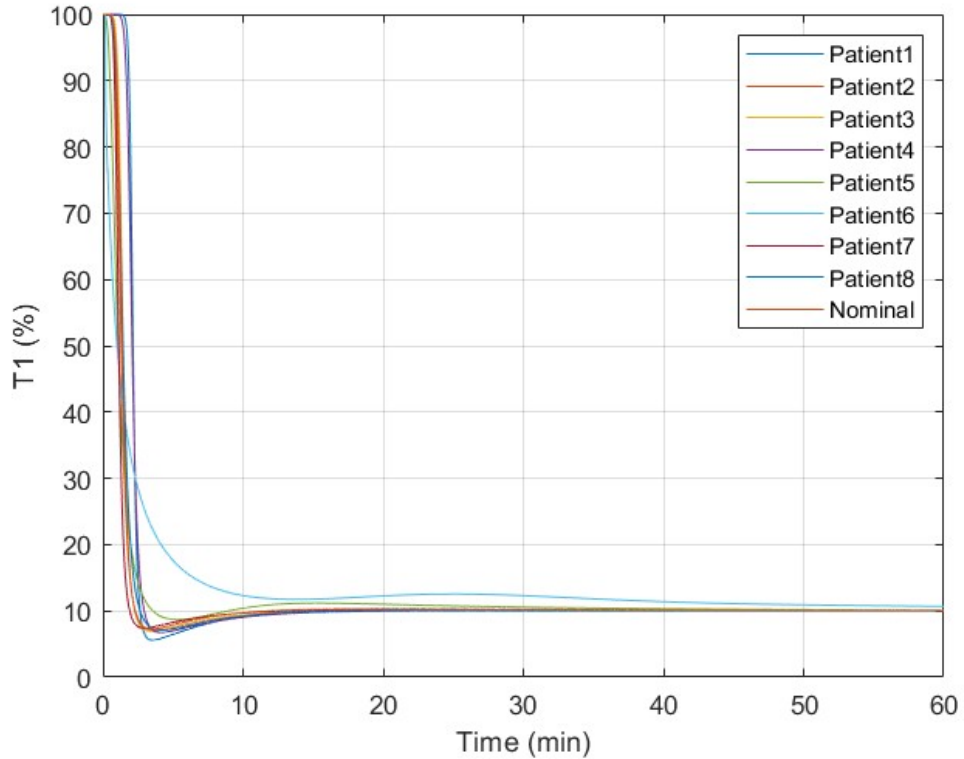


Figure 4.28: All patients response to PID designed with FR tool

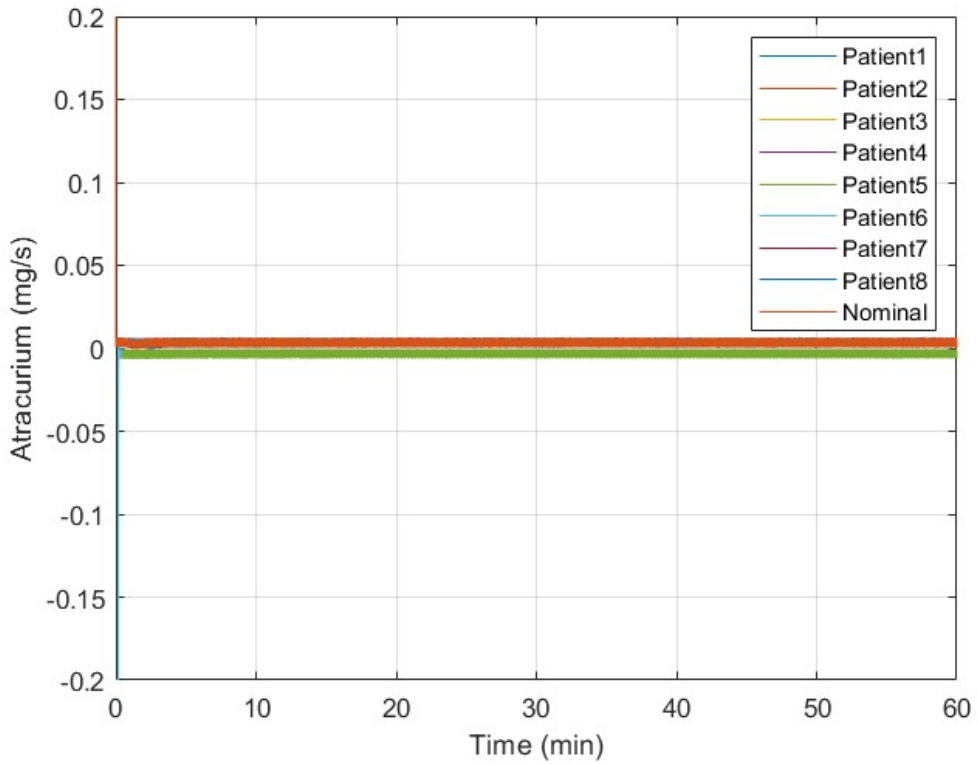


Figure 4.29: Infusion rates of PID designed with FR tool

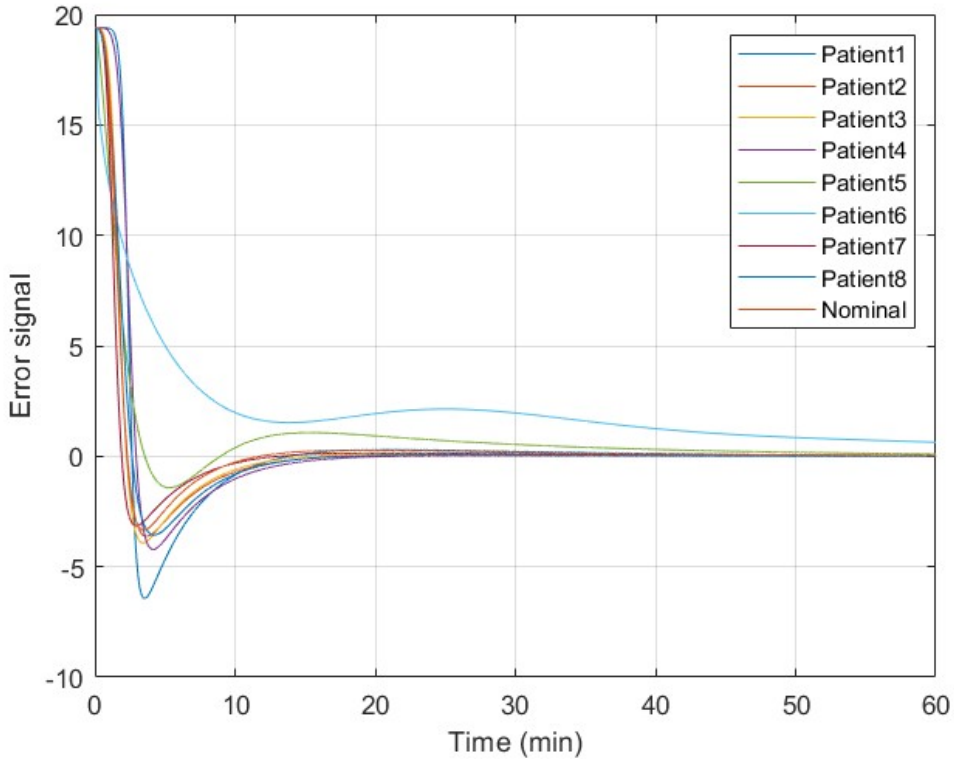


Figure 4.30: Error signal of all patients

#### 4.2.2. IMC Tuning

The IMC was implemented following the algorithm in Section 3.3.2. The first step is to write the controller's transfer function as the inverse of the nominal patient's transfer function:

$$H_{nom}(s) = \frac{0.35556(s + 0.134)}{s^2 + 0.00208s + 2.56 \cdot 10^{-6}} e^{-10s}$$

The controller's transfer function becomes:

$$C(s) = \frac{s^2 + 0.00208s + 2.56 \cdot 10^{-6}}{0.35556(s + 0.134)e^{-10s}}$$

A first-order low-pass filter should be added to make the controller's transfer function proper as the difference between the degree of the controller's nominator and denominator is equal to one. Yet, after testing it was shown that a second-order low-pass filter gives better results:

$$F(s) = \frac{1}{(\lambda s + 1)^2}$$

where  $\lambda$  is chose equal to 180.

The poles of the nominal patient's transfer function are complex conjugates:  $p_1 = -0.00104 - 0.001215j$  and  $p_2 = -0.00104 - 0.001215j$ , with the real part  $R_e = -0.00104$  in the left-half plane. The system's instability is the 10 second delay introduced by the measurement device, approximated using Taylor series approximation:

$$e^{-10s} = 1 - 10s$$

Thus, the invertible part of the system  $\tilde{P}_g(s)$  remains equals to  $H_{nom}(s)$ , while the non-invertible part is represented by the delay approximation  $\tilde{P}_b(s) = 1 - 10s$ .

The final controller's transfer function is:

$$R(s) = \frac{0.148s^2 + 0.0003079s + 3.789 \cdot 10^{-7}}{s^2 + 0.134s}$$

The nominal patient's response is shown in Figure 4.31. This controller has a settling time of 20 minutes, better than the previous controller. When tested on the other patients, it also provides smoother patient responses without undershoots. Similar to the previous controller, patient 6 exceeds the reference value in the first 50 minutes but then stabilizes at the target of 10%, meeting the requirements.

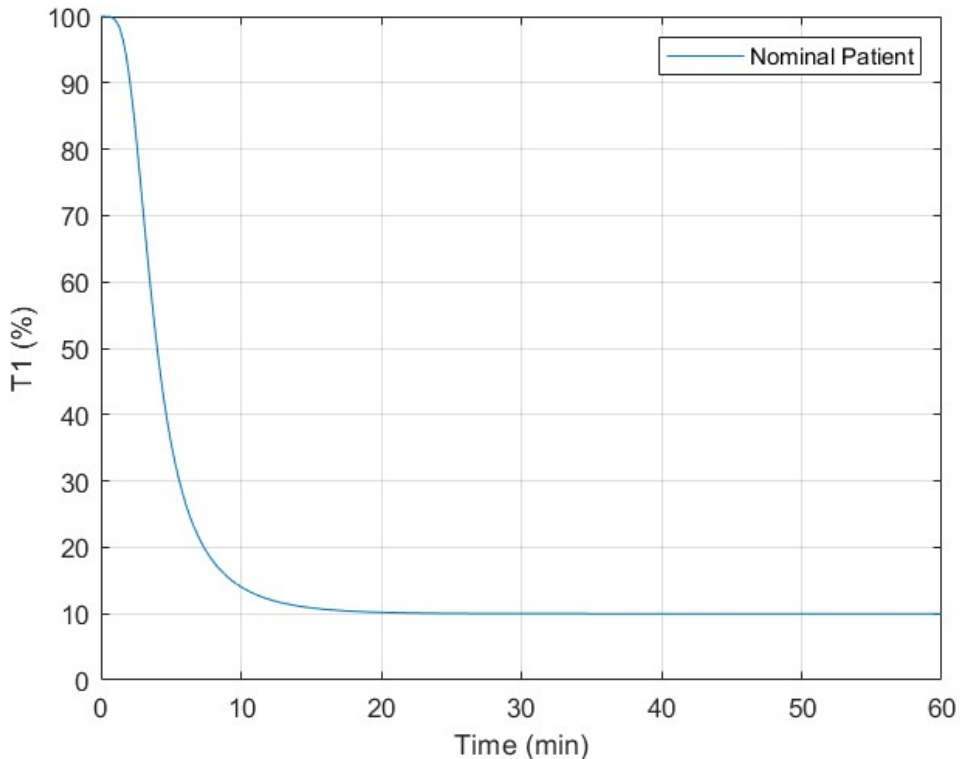


Figure 4.31: Nominal patient's response to IMC control

Also, Figure 4.33 displays the infused drug rates, for most of them this value being around 0.01 mg/sec. Figure 4.34 shows that the controller can minimize the error for most of the patients after one hour.

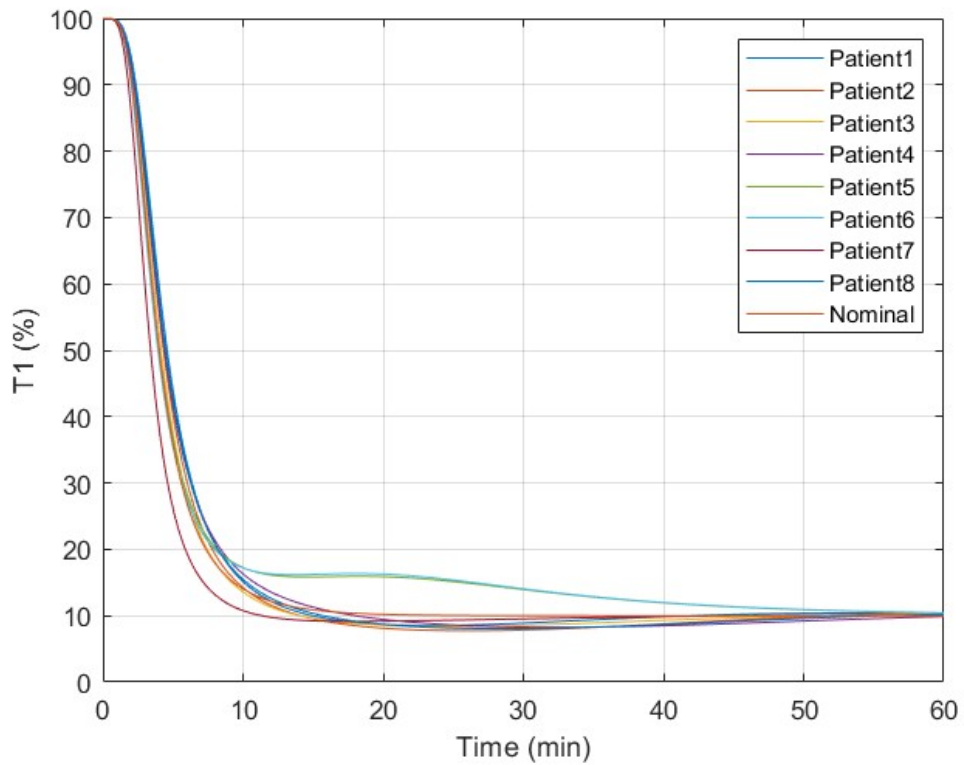


Figure 4.32: All patients response to IMC control

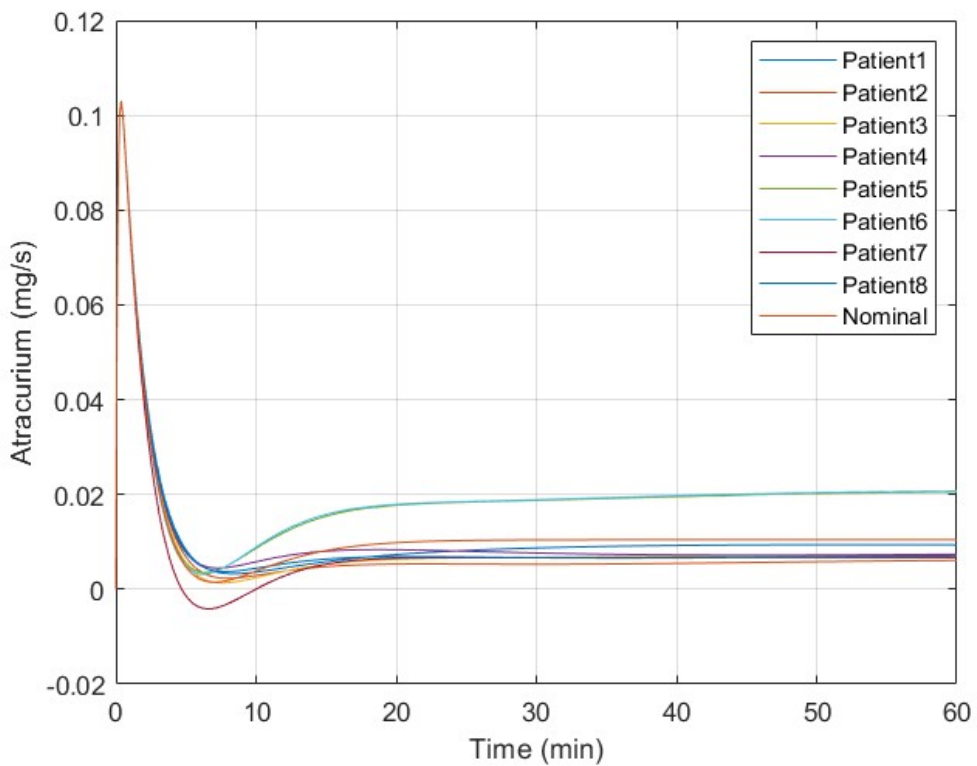


Figure 4.33: Infusion rates of all patients given by IMC

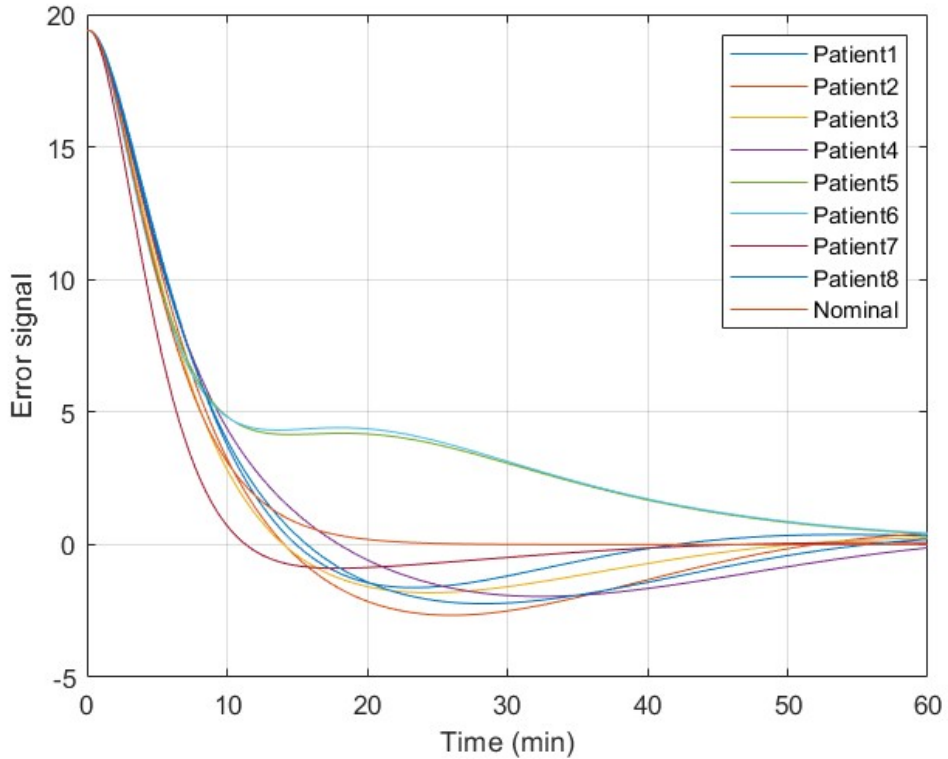


Figure 4.34: Error signals of all patients given by IMC

# **Chapter 5. Conclusions**

## **5.1. Contributions and Achievements**

Control of drug delivery systems poses a manifold of challenges due to its complexity and crucial nature. Modelling and control of such systems in general anaesthesia becomes more important as the number of surgeries increases each year. Advances in medical technology are helping in automating the anaesthesia process. Using feedback control in anaesthesia improves patient safety and comfort and reduces the workload for anaesthesiologists. Despite the success of current controllers in simulations and real surgeries, anaesthesiologists still play a major role.

The main focus of this paper is on hypnosis and neuromuscular blockade, both modeled as single-input single-output (SISO) systems. For hypnosis, the input is propofol, and the output is the Bispectral Index (BIS). A pharmacokinetic-pharmacodynamic (PKPD) model, represents the drug-body interaction, while accounting for daily physiological variations. For neuromuscular blockade, the input is atracurium, and the output is the amplitude of the first twitch in response to stimulation. In this case, Wiener models are enhanced. The Hill function introduces the nonlinearity in both scenarios, converting drug concentration effects into measurable outputs (BIS and T1). This nonlinearity is addressed with a parameter scheduling technique, specifically the inverse of the Hill function, described using nominal patient parameters.

Three control strategies were developed for hypnosis: PID with FR tool, PID-IMC, and MPC. These strategies were based on a nominal patient model and tested on a set of 12 patients to evaluate their responsiveness to intra- and inter-patient variability and disturbance rejection. All controllers showed satisfactory performance. The PID with FR tool showed sudden variations and increased settling times in some patients but maintained BIS within the recommended range of 40-60 and met the 180 second settling time requirement. The IMC provided smoother responses with a settling time of 143 seconds for the nominal patient, although one patient experienced a significant undershoot that was minimized by tuning the filter's time constant. The MPC performed best, with a settling time of 90 seconds, effectively handling variability without undershoots or overshoots. However, disturbance rejection across all controllers was suboptimal, maintaining BIS within a range of 30-70, which requires improvement for patient safety and comfort.

For neuromuscular blockade, two control strategies were developed: PID with an FR tool and IMC. Both strategies were based on a nominal patient model and tested on a group of 8 patients. The PID with FR tool achieved a settling time of 30 minutes for most patients, with minor undershoots. One patient required a settling time of 50 minutes, still within the 60-minute constraint. The IMC showed better handling of variability, reaching the target within 20 minutes for most patients. Two patients had longer settling times, but these were still within acceptable limits.

Overall, the results are satisfactory, though there is room for improvement. IMC

controllers could benefit from further tuning of filter time constant or order, while MPC could improve disturbance rejection by increasing the prediction horizon.

## **5.2. Future Developments**

This work primarily focused on hypnosis and neuromuscular blockade, two of the components of general anaesthesia. The literature presents various studies with promising results, some of which have been implemented in real-world scenarios. Even so, to complete the triad of general anaesthesia, analgesia must also be addressed. Analgesia, which represents the level of pain a patient might experience during surgery, has not been studied as much as hypnosis and neuromuscular blockade. There are few developments in this area in the literature. Developing reliable models and control systems for analgesia will significantly make progress in the automation of general anesthesia.

Moreover, multivariable systems must be considered since all three components of anaesthesia - hypnosis, neuromuscular blockade, and analgesia — interact in the surgical room. Reliable models need to be developed, and extensive studies must be conducted to understand how these components influence each other, aiming for models that closely match the reality.

Also, there is always room for improvement in Single Input Single Output (SISO) models used in general anaesthesia. Patients may not respond consistently to the same drugs due to daily physiological variations. Current PKPD models do not consider such variations, as they depend on parameters like weight, height, age, and gender. Integrating these variations will significantly strengthen the reliability of these systems.

Future work will also involve further tuning of the controllers. To improve disturbance rejection, Kalman filters will be incorporated. The focus will shift towards more advanced control techniques, such as adaptive control, as they offer more optimal responses and better disturbance rejection.

For hypnosis, since the Bispectral Index (BIS) is not the only measure of the depth of anaesthesia, future simulations will include aepEX as an output for comparison with BIS simulations. Different models for propofol parameters will also be tested to compare responses. The ultimate goal is to develop more robust and versatile systems that can adapt to varying patient conditions, thereby enhancing patient safety and comfort.

## Bibliography

- [1] J. G. Meara, A. J. M. Leather, L. Hagander, B. C. Alkire, N. Alonso, E. A. Ameh, S. W. Bickler, L. Conteh, A. J. Dare, J. Davies, E. D. Mérисier, S. El-Halabi, P. E. Farmer, A. Gawande, R. Gillies, S. L. M. Greenberg, C. E. Grimes, R. L. Gruen, E. A. Ismail, T. B. Kamara, C. Lavy, G. Lundeg, N. C. Mkandawire, N. P. Raykar, J. N. Riesel, E. Rodas†, J. Rose, N. Roy, M. G. Shrime, R. Sullivan, S. Verguet, D. Watters, T. G. Weiser, I. H. Wilson, G. Yamey, and W. Yip, “Global surgery 2030: evidence and solutions for achieving health, welfare, and economic development,” *The Lancet*, vol. 386, no. 9993, pp. 569–624, 2015. [Online]. Available: [https://doi.org/10.1016/S0140-6736\(15\)60160-X](https://doi.org/10.1016/S0140-6736(15)60160-X)
- [2] A. Dumas, “The history of anaesthesia,” *Journal of the National Association*, vol. 24, no. 1, pp. 6–9, 1932. [Online]. Available: <https://www.ncbi.nlm.nih.gov/pmc/articles/PMC2625225/pdf/jnma00773-0008.pdf>
- [3] A. TOMA and M. sahib, “A comprehensive review on automated control of anesthesia: Recent methods, challenges and future trends,” *Wasit Journal for Pure sciences*, vol. 2, pp. 291–315, 06 2023.
- [4] I. Nascu and E. Pistikopoulos, “Modeling, estimation and control of the anaesthesia process,” *Computers Chemical Engineering*, vol. 107, 02 2017.
- [5] C. L. Beck, “Modeling and control of pharmacodynamics,” *European Journal of Control*, vol. 24, pp. 33–49, 2015, sI: ECC15. [Online]. Available: <https://www.sciencedirect.com/science/article/pii/S0947358015000618>
- [6] R. Hodrea, R. Morar, I. Nascu, and H. Vasian, “Modeling of neuromuscular blockade in general anesthesia,” in *2013 8TH INTERNATIONAL SYMPOSIUM ON ADVANCED TOPICS IN ELECTRICAL ENGINEERING (ATEE)*, 2013, pp. 1–4.
- [7] A. Hagenblad, L. Ljung, and A. Wills, “Maximum likelihood identification of wiener models,” *IFAC Proceedings Volumes*, vol. 41, no. 2, pp. 2714–2719, 2008, 17th IFAC World Congress. [Online]. Available: <https://www.sciencedirect.com/science/article/pii/S1474667016393624>
- [8] J. Schüttler and H. Schwilden, Eds., *Modern Anesthetics*, ser. Handbook of Experimental Pharmacology. Berlin, Heidelberg: Springer, 2008, vol. 182. [Online]. Available: <https://link.springer.com/book/10.1007/978-3-540-74806-9>
- [9] C. M. Ionescu, D. Copot, M. Neckebroek, and C. I. Muresan, “Anesthesia regulation: Towards completing the picture,” in *2018 IEEE International Conference on Automation, Quality and Testing, Robotics (AQTR)*, 2018, pp. 1–6.

- [10] Y. He, S. Peng, M. Chen, Z. Yang, and Y. Chen, "A transformer-based prediction method for depth of anesthesia during target-controlled infusion of propofol and remifentanil," *IEEE transactions on neural systems and rehabilitation engineering : a publication of the IEEE Engineering in Medicine and Biology Society*, vol. PP, 08 2023.
- [11] S. G. J. M. H. A. J. Surbhi Mathur, Jashvin Patel, "Bispectral index," <https://www.ncbi.nlm.nih.gov/books/NBK539809/>, accessed: 2024-02-16.
- [12] J. Liu, K. Dong, Y. Sun, I. Kakkos, F. Huang, G. Wang, P. Qi, X. Chen, D. Zhang, A. Bezerianos, and Y. Sun, "Progress of brain network studies on anesthesia and consciousness: Framework and clinical applications," *Engineering*, vol. 20, pp. 77–95, 2023. [Online]. Available: <https://www.sciencedirect.com/science/article/pii/S2095809921005269>
- [13] L. Merigo, F. Padula, N. Latronico, M. Paltenghi, and A. Visioli, "Optimized tuning of an imc scheme for depth of hypnosis control," in *2019 18th European Control Conference (ECC)*, 2019, pp. 203–208.
- [14] G. Rodney, P. Raju, and S. Brull, "Neuromuscular block management: evidence-based principles and practice," *BJA Education*, vol. 24, 11 2023.
- [15] D. J. S. Danielle Cook, "Neuromuscular blockade," <https://www.ncbi.nlm.nih.gov/books/NBK538301/>, accessed: 2024-04-27.
- [16] I. Nascu, E. Pistikopoulos, and I. Nascu, "Hybrid multiparametric model predictive control with application to the neuromuscular blockade," 05 2018, pp. 1–6.
- [17] J. Viby-Mogensen, "Monitoring neuromuscular function in the intensive care unit," *Intensive care medicine*, vol. 19 Suppl 2, pp. S74–9, 02 1993.
- [18] "Muscle relaxants;; reversal and the use of peripheral nerve stimulators," [www.perioperativecpd.com/](http://www.perioperativecpd.com/), accessed: 2024-04-27.
- [19] M. Martins da Silva, T. Mendonça, and T. Wigren, "Nonlinear adaptive control of the neuromuscular blockade in anesthesia," in *2011 50th IEEE Conference on Decision and Control and European Control Conference*, 2011, pp. 41–46.
- [20] M. Guen, N. Liu, and J. Selim, "Computer-assisted iv anesthesia: Still a future?" *Current Anesthesiology Reports*, vol. 13, pp. 1–9, 07 2023.
- [21] C. Csajka and D. Verotta, "Pharmacokinetic-pharmacodynamic modelling: history and perspectives," *Journal of Pharmacokinetics and Pharmacodynamics*, vol. 33, no. 3, pp. 227–79, Jun. 2006, epub 2006 Jan 11.
- [22] M. Schiavo, F. Padula, N. Latronico, M. Paltenghi, and A. Visioli, "On the practical use of a pid-based control scheme for automatic control of general anesthesia," in *2022 IEEE Conference on Control Technology and Applications (CCTA)*, 2022, pp. 1105–1110.

- [23] B. L. Moore, L. D. Pyeatt, and A. G. Doufas, “Fuzzy control for closed-loop, patient-specific hypnosis in intraoperative patients: A simulation study,” in *2009 Annual International Conference of the IEEE Engineering in Medicine and Biology Society*, 2009, pp. 3083–3086.
- [24] D. Copot, F. Kusse, M. Ghita, M. Ghita, M. Neckebroek, and A. Maxim, “Distributed model predictive control for hypnosis-hemodynamic maintenance during anesthesia,” in *2019 23rd International Conference on System Theory, Control and Computing (ICSTCC)*, 2019, pp. 638–643.
- [25] A. Pawlowski, M. Schiavo, N. Latronico, M. Paltenghi, and A. Visioli, “Experimental results of an mpc strategy for total intravenous anesthesia,” *IEEE Access*, vol. 11, pp. 32 743–32 751, 2023.
- [26] A. Khaqan and R. A. Riaz, “Depth of hypnosis regulation using nonlinear control approach,” in *2016 IEEE International Conference on Electro Information Technology (EIT)*, 2016, pp. 0100–0104.
- [27] E. Furutani, Y. Nishigaki, C. Kanda, T. Takeda, and G. Shirakami, “Hypnosis control based on the minimum concentration of anesthetic drug for maintaining appropriate hypnosis,” in *2013 35th Annual International Conference of the IEEE Engineering in Medicine and Biology Society (EMBC)*, 2013, pp. 3483–3486.
- [28] J. Silva, T. Mendonça, and P. Rocha, “Improving tci control for the automatic delivery of rocuronium,” in *2020 28th Mediterranean Conference on Control and Automation (MED)*, 2020, pp. 905–908.
- [29] T. Mendonça, H. Magalhães, J. M. Lemos, P. Rocha, and S. Esteves, “Multiple model adaptive control of neuromuscular blockade: Design guidelines and clinical cases,” in *2007 European Control Conference (ECC)*, 2007, pp. 2541–2546.
- [30] R. Hodrea, I. Nascu, I. Nascu, R. De Keyser, and H. Vasian, “Epsac versus pid control of neuromuscular blockade,” in *2014 IEEE International Conference on Automation, Quality and Testing, Robotics*, 2014, pp. 1–6.
- [31] F. Taheriyani, M. s. Ghafourian, and A. Noori, “Applying ga optimization algorithm for interval type-2 fuzzy logic controller parameters of multivariable anesthesia system,” in *Electrical Engineering (ICEE), Iranian Conference on*, 2018, pp. 1613–1618.
- [32] “The pid controller theory explained,” <https://www.ni.com/en/shop/labview/pid-theory-explained.html#section--2054068860>, accessed: 2024-04-28.
- [33] C. Muresan, “Lecture 10: Internal model control,” Lecture, Technical University of Cluj-Napoca, 2023, control Engineering II, University Lecture.
- [34] L. Wang, “Model predictive control: Design and implementation using matlab (t-3),” in *2009 American Control Conference*, 2009, pp. 1–21.
- [35] I. Nascu, I. Nascu, C. M. Ionescu, and R. De Keyser, “Adaptive epsac predictive control of the hypnotic component in anesthesia,” in *Proceedings of 2012 IEEE International Conference on Automation, Quality and Testing, Robotics*, 2012, pp. 103–108.

- [36] M. Sahinovic, M. Struys, and A. Absalom, “Clinical pharmacokinetics and pharmacodynamics of propofol,” *Clinical Pharmacokinetics*, vol. 57, no. 12, pp. 1539–1558, Dec 2018. [Online]. Available: <https://www.ncbi.nlm.nih.gov/pmc/articles/PMC6267518/>
- [37] I. Nascu, C. M. Ionescu, I. Nascu, and R. De Keyser, “Evaluation of three protocols for automatic doa regulation using propofol and remifentanil,” in *2011 9th IEEE International Conference on Control and Automation (ICCA)*, 2011, pp. 573–578.

## **Appendix A. Published Papers**

A.R. Dafinoiu, I. Nașcu, "PID control for intravenous depth of anesthesia", *AQTR, Cluj-Napoca, 2024*